SPAWAR

Systems Center
San Diego

TECHNICAL DOCUMENT 3027
April 1998

Multifunctional Antenna Systems FY 97 Technology Development

T. Q. Ho
R. C. Adams
W. I. Henry
S. M. Hart

TECHNICAL DOCUMENT 3027
April 1998

Multifunctional Antenna Systems FY 97 Technology Development

T. Q. Ho
R. C. Adams
W. I. Henry
S. M. Hart

Systems Center San Diego

Space and Naval Warfare Systems Center
San Diego, CA 92152–5001

SPACE AND NAVAL WARFARE SYSTEMS CENTER
San Diego, California 92152–5001

H. A. Williams, CAPT, USN
Commanding Officer

R. C. Kolb
Executive Director

ADMINISTRATIVE INFORMATION

The work detailed in this report was performed for the Office of Naval Research by Advanced Electromagnetics Technology Branch, Code D856, Space and Naval Warfare (SPAWAR) Systems Center, San Diego. Funding for this project was provided under program element 0602232N.

Released by
D. W. Tam, Head
Advanced Electromagnetics
Technology Branch

Under authority of
C. J. Sayre, Head
Electromagnetics &
Advanced Technology
Division

SB

PREFACE

In FY 97, we conducted two tasks. The objective of the first task was to develop new directive antenna system concepts for satellite communications (SATCOM) applications. The focus of the second task was to develop novel line-of-sight (LOS) antenna concepts and electronics to support the Multifunction Electromagnetic Radiating System Advanced Technology Demonstration (MERS ATD).

CONTENTS

Figures

Tables

TASK 1
DIRECTIVE ANTENNA SYSTEM CONCEPTS FOR SATCOM

1. INTRODUCTION

The current satellite communications (SATCOM) systems on U.S. combatants use mechanically steered antennas to transmit and receive circularly polarized signals from the Ultra High Frequency (UHF) to the Extremely High Frequency (EHF) band (Space and Naval Warfare Systems Command, 1991). In certain applications (e.g., UHF, Super High Frequency (SHF) SATCOM), the combatant may require two antennas due to the placement below the topmost level and blockage by the forward superstructure. One antenna is located on the starboard side and the other on the port. The need for greater bandwidth in the system and smaller size for the antenna encourages the use of much higher frequencies. A smaller size antenna would also permit it to be located on the topmost part of the mast. Another advantage is that the decreased size reduces the radar cross section and the threat that the ship faces in a hostile environment.

The use of phased-array technology to implement SATCOM functions is advantageous over the conventional parabolic dish antenna from several standpoints. Using one antenna aperture for several functions is desirable because it conserves very valuable space on the crowded topside of surface ships, providing greater capability while reducing weight and moment. Flexibility in the implementation of multiple beams steered to several satellites can be enhanced via phased-array technology. Since this technology allows the utilization of conformal embedded antenna elements, the radar cross section (RCS) signature of the aperture can be greatly reduced. These are some of the key requirements for future surface combatants. Additionally, below-deck electronics can enhance reliability. Maintenance costs may be reduced without the need for gimbals and other mechanical devices exposed to the sea's hostile environment. In FY 97, we examined the possibility of using phased-array antenna technology to implement both UHF SATCOM and International Maritime Satellite (INMARSAT) functions. The objective of this study is to develop different antenna technology options for implementation in the near future. Our approach in this study is based on active phased-array antenna technology with a 45° tilted superstructure.

2. SYSTEM REQUIREMENTS

Currently, the Navy is using/planning various frequency bands for SATCOM functions. The systems may include UHF, INMARSAT, GPS, DSCS, GBS, MILSTAR, and many others. As mentioned before, our focus in FY 97 was at the lower band systems, specifically UHF and INMARSAT.

The requirements for two antenna systems, the UHF SATCOM and the INMARSAT are presented in table 1.

Table 1. Requirements for SATCOM systems in the UHF and L-bands.

	UHF SATCOM	INMARSAT
Frequency	244 to 270 MHz (downlink)	1525.0 to 1545.0 MHz (downlink)
	292 to 318 MHz (uplink)	1626.5 to 1646.5 MHz (uplink)
Polarization	RH Circular, Full	RH Circular, Full
Gain	12 dBi Min @ 305 MHz	21.8 dBi (Tx), 21.1 dBi (Rx)
Pattern		
Elevation	Horizon to Zenith	Horizon to Zenith
Azimuth	360°	360°

The INMARSAT satellite provides communications for both land and sea systems. The first INMARSAT II was launched in October 1990. The first INMARSAT III was launched in April 1996. Shipboard antennas for INMARSAT are on the DDG 69 and some follow-ons.

There are other frequency bands that current or future SATCOM systems will use. Table 2 shows some of the key antenna requirements.

Table 2. Characteristics of other SATCOM systems.

	EHF	GBS	DSCS
Frequency (GHz)			
Uplink	43.5 to 45.5	30 to 31	7.9 to 8.4
Downlink	20.2 to 21.2	20.2 to 21.2 (mil)	7.25 to 7.75
		19.2 to 20.2 (com)	
Polarization	RH Circular	LH or RH Circular	LH (D) RH (U)
Gain (dBi)	48.5 (U) 41.5 (D)		37.5 min.
G/T (dB/K)		16.5	12.5

3. DESIGN CONSIDERATIONS

Operating frequency is one of the key parameters that sets the overall size for the array. The gain requirements largely determine the number of elements used in the aperture. The polarization requirements determine the type and construction of the elements. A SATCOM system commonly requires circular polarization to reduce fading of a signal propagating through the ionosphere.

Since it is desired that there will be only one SATCOM aperture located at the highest point on the combatant, the radiation pattern must extend to a full 360° in azimuth. The requirement that the radiation pattern be steerable from horizon to zenith could be met by having the array tilted at a 45° angle from the vertical. Such a choice would minimize scan/roll-off losses. The greater attenuation of a signal propagating through the atmosphere at the horizon compared to that at zenith indicates that the array could be tilted at an angle less than 45°. The need to have a full 360° coverage in azimuth probably implies that four or six panels would be needed. Another possible implementation is a conical structure that has no junctions between panels. In either case, tradeoff studies in RCS signature need to be conducted before final implementation.

Each one of the SATCOM systems above has the requirement of being able to steer the beam from horizon to zenith and 360° in azimuth. The described analysis techniques could be applied to these systems as well.

4. SYSTEM ARCHITECTURE

4.1 CONCEPTUAL DESIGNS

Two antenna system concepts have been developed to meet the requirements of transmit and receive. They differ in the numbers of panels and diplexers used and in the types of elements employed. In each system, the same element serves the dual role of transmit and receive. Figure 1 illustrates these concepts as the UHF and INMARSAT SATCOM arrays.

In the first conceptual design, a common antenna element is used. The bandwidth must be wide enough to accommodate both the UHF (244 to 318 MHz) and INMARSAT (1525 to 1650 MHz) frequencies. Additionally, it must satisfy the polarization requirements for these systems. The antenna element will have a common feed so that both UHF and INMARSAT signals can be fed simultaneously to the antenna panel. The signal distribution partitions the UHF from the INMARSAT signal. One possible implementation is the utilization of the multiplexers. In this configuration, a diplexer can be used to separate transmit and receive in each band. A third-tier diplexer is also needed to combine the two bands, that is, UHF and L-band signals going to the same antenna element. This concept has the advantage of requiring only one antenna panel with a single set of antenna elements. The drawback is that the choice of elements is restricted due to the large bandwidth required.

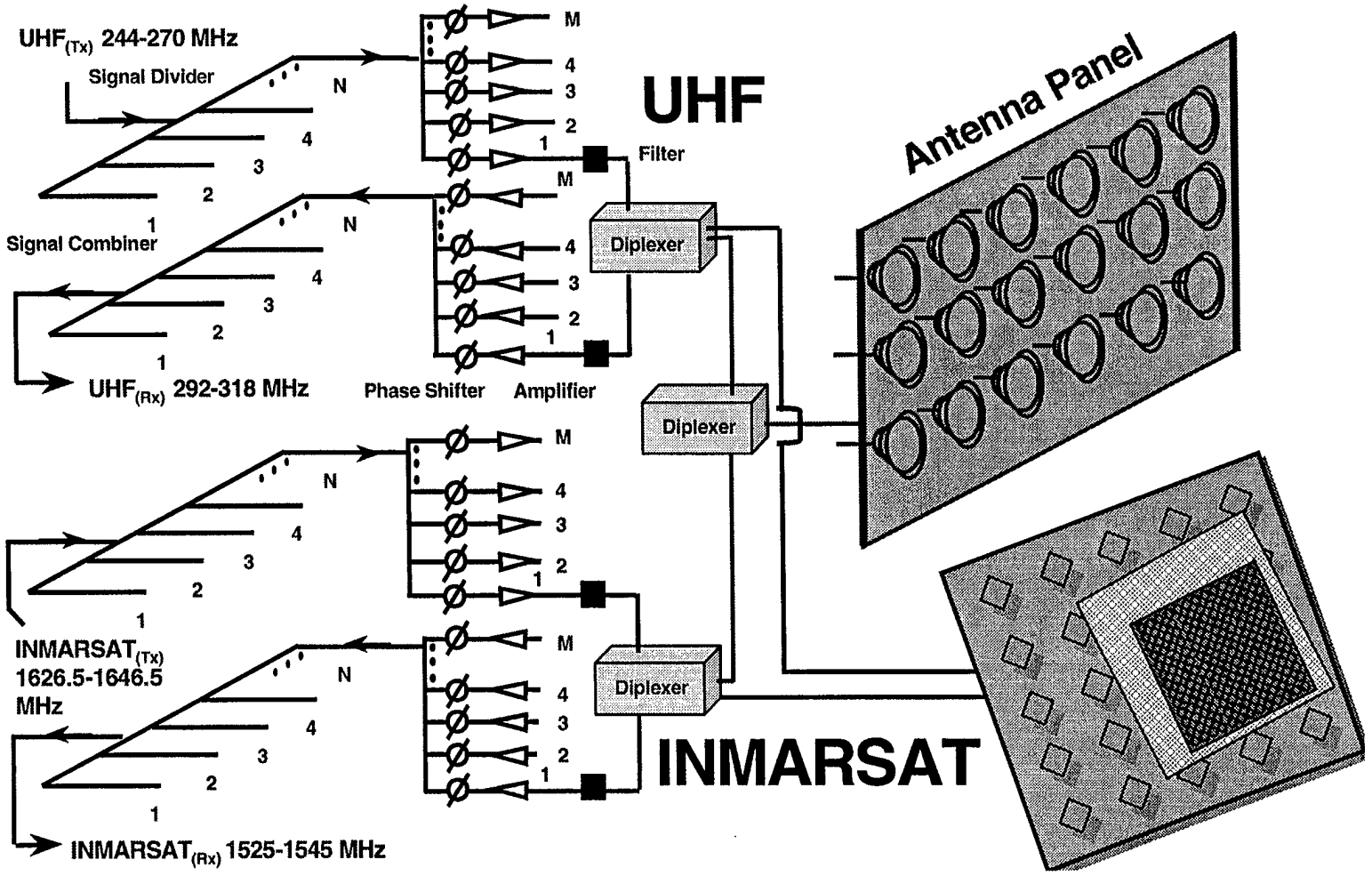

Figure 1. Integrated Satellite Communications System (SATCOM) architecture.

The second concept is to separate the panels into two bands. One possible implementation is that two antenna panels are located at the same location, but one is on top of the other. The elements designed to the UHF band are in the large panel that forms the back of the array. The upper elements are for the INMARSAT function. A low-pass, frequency-selective surface (Ho, 1994a; 1994b) is placed between the UHF and INMARSAT antenna panels. The Frequency Selective Surface (FSS) serves as the ground plane for the INMARSAT panel while being transparent at UHF. This property allows the antenna to propagate an UHF signal. The laminated antenna panel has two feed points in this configuration. One feed point is for UHF and the other is for INMARSAT. This type of implementation has the advantage of easing the restriction on the type of element to be used. Narrowband elements such as patches are applicable. In FY 97, we focus our antenna study based on this concept.

4.2 LINK BUDGET

The primary factor that determines the size of the array is the need for high gain in the antenna pattern. The overall gain of the INMARSAT array must be at least 21.8 dBi. The corresponding gain for UHF is 12.0 dBi. The quantity derived from the analysis of the array presented below is the directivity related to the gain by the efficiency of the antenna and feed network. Table 3 presents the link budget. All quantities are in dBi.

The peak directivity needed to provide for the gain while accommodating various losses is largely determined by the number and arrangement of the elements in the array. This study indicated that a directivity of 27.2 dBi and 17.4 dBi is needed for INMARSAT and UHF, respectively, to meet the overall antenna requirements. The analysis is based on a 45° tilted superstructure.

Table 3. Power link budgets for two SATCOM systems.

Parameter	Description	INMARSAT	UHF
Peak directivity	Antenna analysis	27.20	17.40
Scan loss	45°	-1.51	-1.51
Rolloff/Grating lobes	Pattern simulation	-1.60	-1.60
Squint loss	Pattern analysis	-0.15	-0.20
Antenna efficiency	75%	-1.25	-1.25
Feed loss	VSWR/Ohmic/I.L.	-0.50	-0.40
Phase error	10° rms phase error	-0.12	-0.12
Amplitude error	Estimate	-0.05	0.05
Phase-Shift quantization error	4 to 6-bit phase shifter	0.08	-0.08
Failure	5% element failure	-0.22	-0.22
Minimum Gain		21.82	12.07

5. ANTENNA THEORY

5.1 RADIATING ELEMENTS

Since their introduction by Munson in 1974, microstrip patches have found a variety of uses as antennas. The small size and ability to conform to many surfaces favor the use of patches in many applications. Patches are generally narrowband. The resonant frequency of a patch depends upon its physical dimensions such as length, width, and distance between the element and ground plane, shape, and dielectric constant of the substrate. Generally, the dimensions of the patch (either length for a square or diameter for a circular) are approximately one-half the resonant wavelength. The bandwidth of efficient radiation is usually only a few percent of the device's resonant frequency.

A typical design for a microstrip patch is a dielectric substrate between a ground plane and a thin film of metal. The shape of the film is dictated by the application. Rectangles and circles are the most common shapes. The thickness of the dielectric substrate is usually much less than the length or width of the film. The feed mechanism is often either microstrip lines or coax (Elliot, 1981). The polarization of the radiation is dictated by the feeds. Exciting two orthogonal modes in phase quadrature can attain circular polarization. The sign of the relative phase determines the polarization handedness (Hall, 1995). In theory, a figure of merit for determining the degree of circular polarization is the relative power in the theta and phi components of the far field. In practice, the axial ratio, the difference between signals in two orthogonal polarizations, is the figure of merit.

In this study, we used the Maxwell Eminence (1995) to study the properties of the antenna elements. This computer code, which applies the finite element method to solve Maxwell's equations, was used to model both square and circular patches. For each design, the calculations included the impedance of the antenna, the total power radiated to infinity, and the radiation pattern. The primary method of determining the radiation pattern was the use of the real and imaginary parts of the three components of the electric fields. Some of the results were validated with experimental data (Kishk and Shaffai, 1986). The feed lines were modeled so that the impedance of the line was 50 Ω. The inner and outer cylinders were assumed to be perfect metals. Various cases were examined for radiation properties at both UHF and L-band frequencies. The materials under investigation include Honey Comb (1.07), Duroid (2.2), FR4 (4.2), and Alumina (10). The utilization of larger dielectric constants allows the dimensions to decrease for a given resonant frequency.

5.2 ANTENNA ARRAYS

Once the real and imaginary parts of the electric fields have been calculated, theory can be used to predict the array's performance. The assumption used in all of the calculations presented below is that each of the elements does not affect any of the adjacent elements. The mutual coupling is negligible. This allows the electric field of the array to be calculated as the weighted sum of the individual elements. The radiated power is proportional to the absolute square of the electric field.

If each element is located in a rectangular grid in the x-y plane and separated from the adjacent element by a distance, a, the field of the array is given by:

Field of array = field of element X

$$\sum A_m \exp(j\, k\, a\, m \sin(\theta) \cos(\phi) + j\delta_m) \; X \sum A_n \exp(j\, k\, a\, n \sin(\theta) \sin(\phi) + j\delta_n), \qquad (1)$$

where k is the wave number, θ and ϕ are the elevation and azimuth angles of the observer, and A and δ_n are the amplitude and phase of the input to each one of the elements. The role of the amplitude distribution is primarily to reduce side lobes. If the amplitude of the current to each element is the same, the beamwidth of the array is minimized but the level of the side lobes is often high. An amplitude distribution with the maximum current at the center of the array and at a minimum at the edges minimizes the side lobes while increasing the beamwidth a small amount. The phase of the input current serves to minimize the beamwidth and to steer the beam to a desired elevation, θ_o, and azimuth angle, ϕ_o. The phase distribution that steers the maximum of the beam is given by:

$$\delta_m = -k\, a\, m \sin(\theta_o) \cos(\phi_o) \text{ and } \delta_n = -\, k\, a\, n \sin(\theta_o) \sin(\phi_o). \qquad (2)$$

These phase shifts were quantized in units of 22.5°, which simulates the action of a 4-bit phase shifter.

A cosine taper amplitude signal distribution was also used in this study. This distribution has the maximum at the center of the antenna array and minimum at the edges. Mathematically, if the cosine taper and equation (2) are used, the sums in equation (1) can be expressed in closed form. In general, the beamwidth decreases with an increasing number of elements. It is important that the spacing of the elements be less than half the wavelength. If this condition is not met, secondary maxima may rise to unacceptably high levels.

Steering the beam to angles away from the maximum of each of the elements (e.g., the z-axis if the elements are in the x-y plane) typically causes a broadening of the beam and a distribution of some of the power from the maximum to other elevation angles. The maximum still occurs at the angle at which the beam is steered but the amplitude is reduced and the level of the side lobes is increased. The loss of power from the maximum of the beam increases with increasing elevation angle, but has a complicated dependence on the number of elements.

6. NUMERICAL RESULTS

Figure 2 presents the directivity versus the number of elements for square arrays when square and circular patches are utilized. In both cases, the frequency of operation was 305 MHz. The spacing between the antenna elements was 50.8 cm. In each case, substrate of different materials was used to examine their effects upon the radiation patterns. The ordinate represents directivity (dBi) and the abscissa represents the array size. Note that there are two units for array size. The top unit is N, where N x N is the number of elements. The bottom unit is Log (# of elements). For small numbers of elements in the array, the directivity of the individual element dominates the overall value. As the number of elements increases, the directivity of the array in dBi is proportional to the logarithm of the number of elements. For a large array, there is a small difference due to the type of material used.

From these design curves we can determine the required directivity for each application. The directivity for arrays of 25 and 169 square patches is 19.9 and 27.9 dBi, respectively. This directivity determines the minimum number of elements to be used in the UHF and INMARSAT designs.

The steering of the antenna array can be accomplished by adjusting the phase shifts of each element. Figures 3, 4, 5, 6, and 7 present the radiation patterns for UHF and INMARSAT arrays when different design options of square and circular elements were utilized. In these cases the radiation patterns of the antenna array were steered from 0° to 10°, 20°, 30°, and 45°. Since the panel is tilted 45° from the vertical, a 45° angle steered up from the baseline would represent zenith, and a similar angle steered down would represent the horizon. In other words, these design options can be utilized to steer the beam from horizon to zenith without any obstruction. The differences between the results in the above figures consist of the type of element used (square patches for figures 3 and 4 and circular patches for figures 5 and 6), taper (uniform or cosine), numbers of elements (25 or 169), frequency of operation (305 or 1600 MHz), and dielectric constant and dimensions of the antenna element. The figures also include the phase values of the phase shifters in these options. Note that the phase shifters are 4-bit.

For each of the graphs of the power versus angle, the plot is normalized to the maximum of the radiation pattern. Steering the beam from $\theta = 0°$ causes an energy transfer from the maximum to the side lobes. The use of substrate material with a dielectric constant larger than 1 allows the dimensions of the element to be decreased while retaining the same resonant frequency. The use of higher dielectric material has the drawback of decreasing efficiency with the advantage of reducing the size. This application-dependent factor should be a key in future antenna designs.

The use of the uniform taper (figures 3 and 4) causes the beamwidth to be minimized while increasing the side lobes. The cosine taper (figures 5 and 6) minimizes the side lobes while increasing the beamwidth. This is the main reason why many current antenna systems are using this second type of signal distribution. Figure 7 presents the radiation patterns of the UHF array when the array is steered conically. This can be accomplished by choosing different phase-shifter values, as indicated in figure 7. The phase shifts to each element changed accordingly. This figure demonstrates the ability of the array to execute a searching scan. A similar study has also been done with the INMARSAT array.

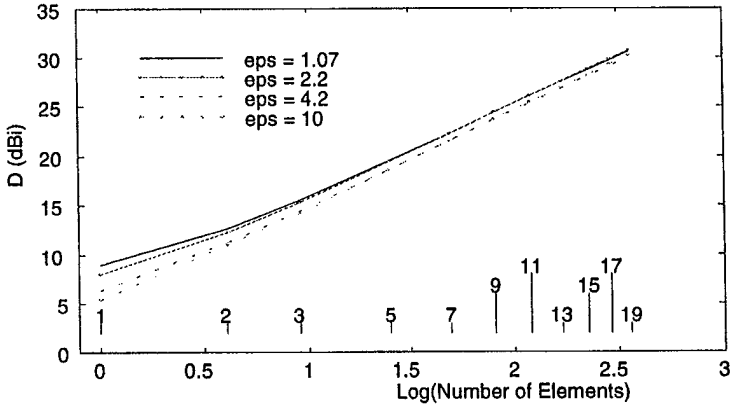

Rectangular Patches

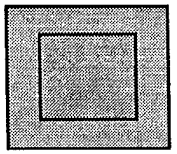

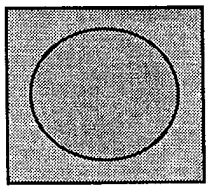

Circular Patches

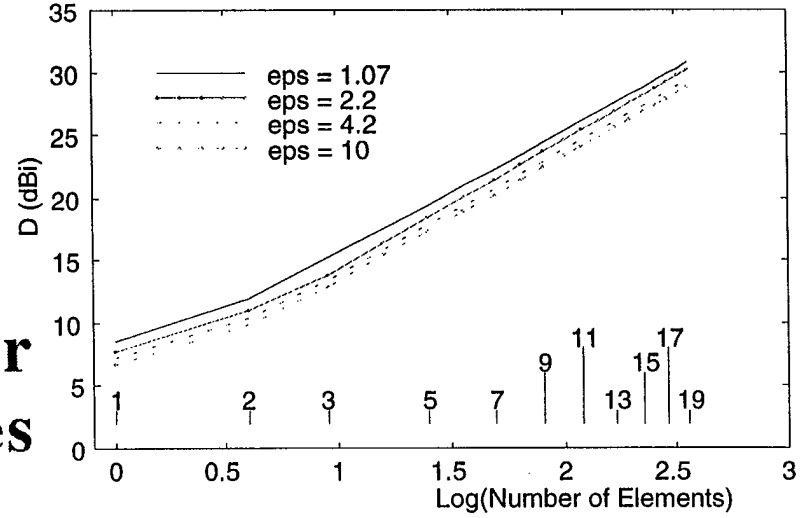

Figure 2. Directivity versus number of elements.

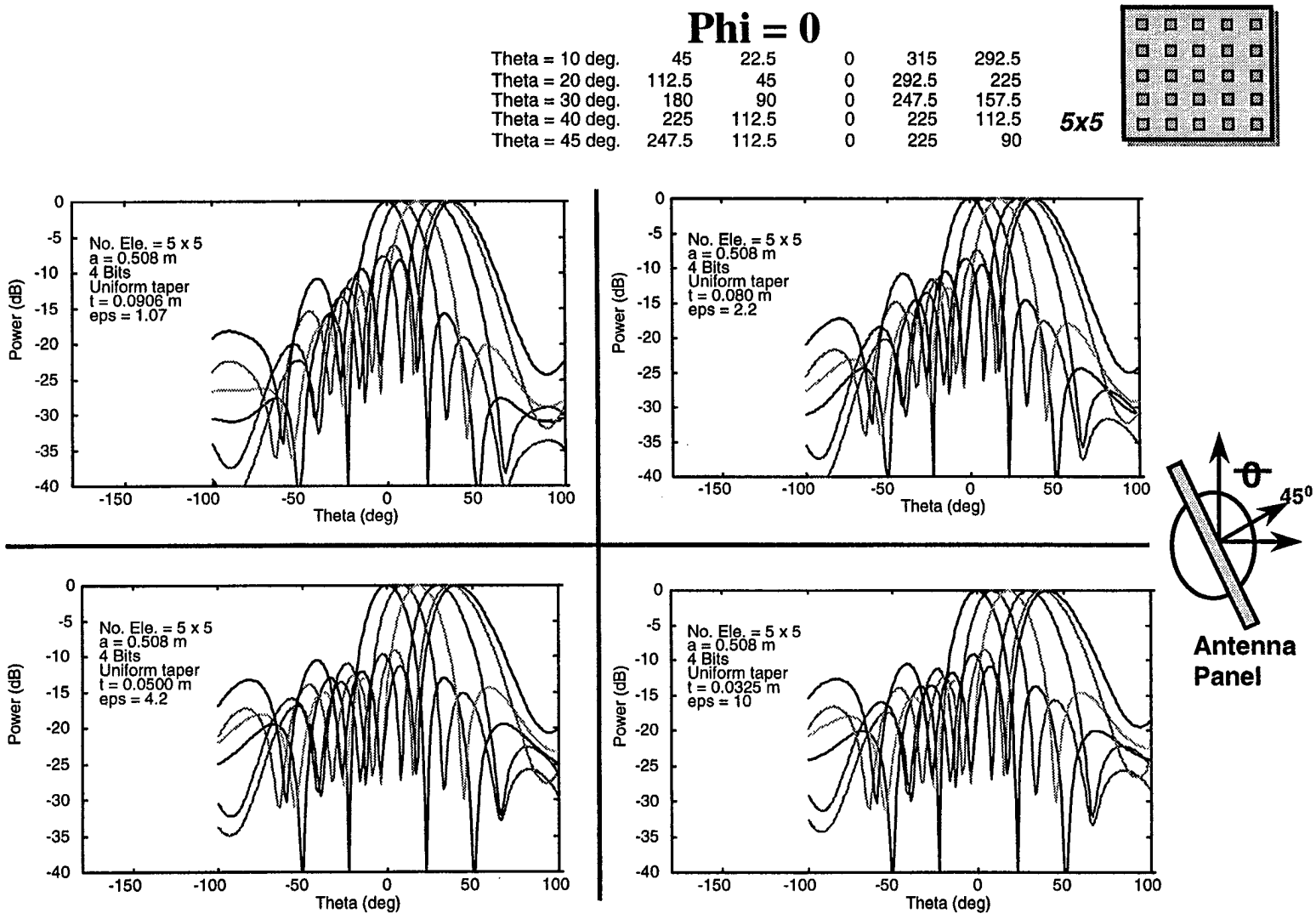

Figure 3. Steering of UHF array.

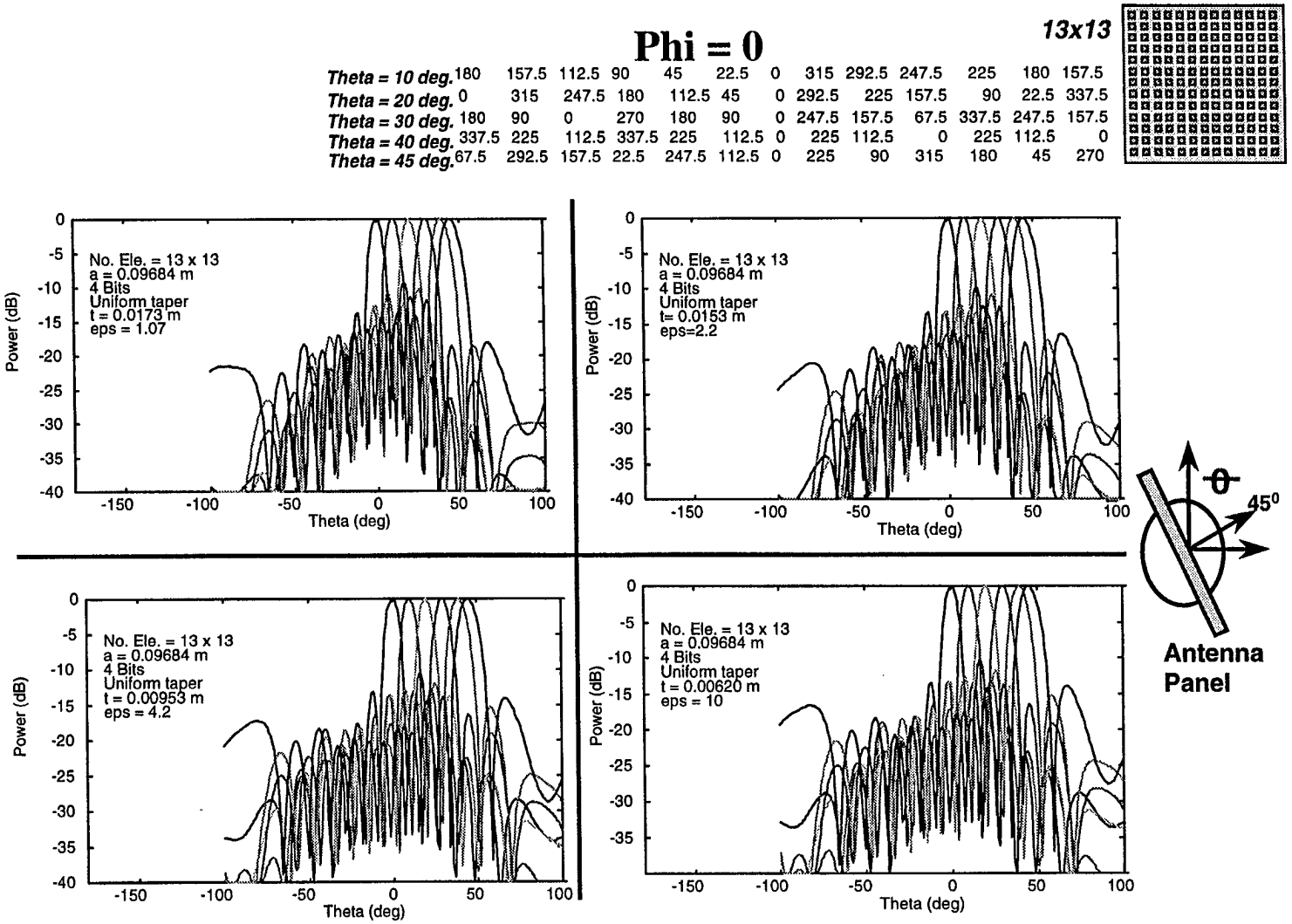

Figure 4. Steering of INMARSAT array.

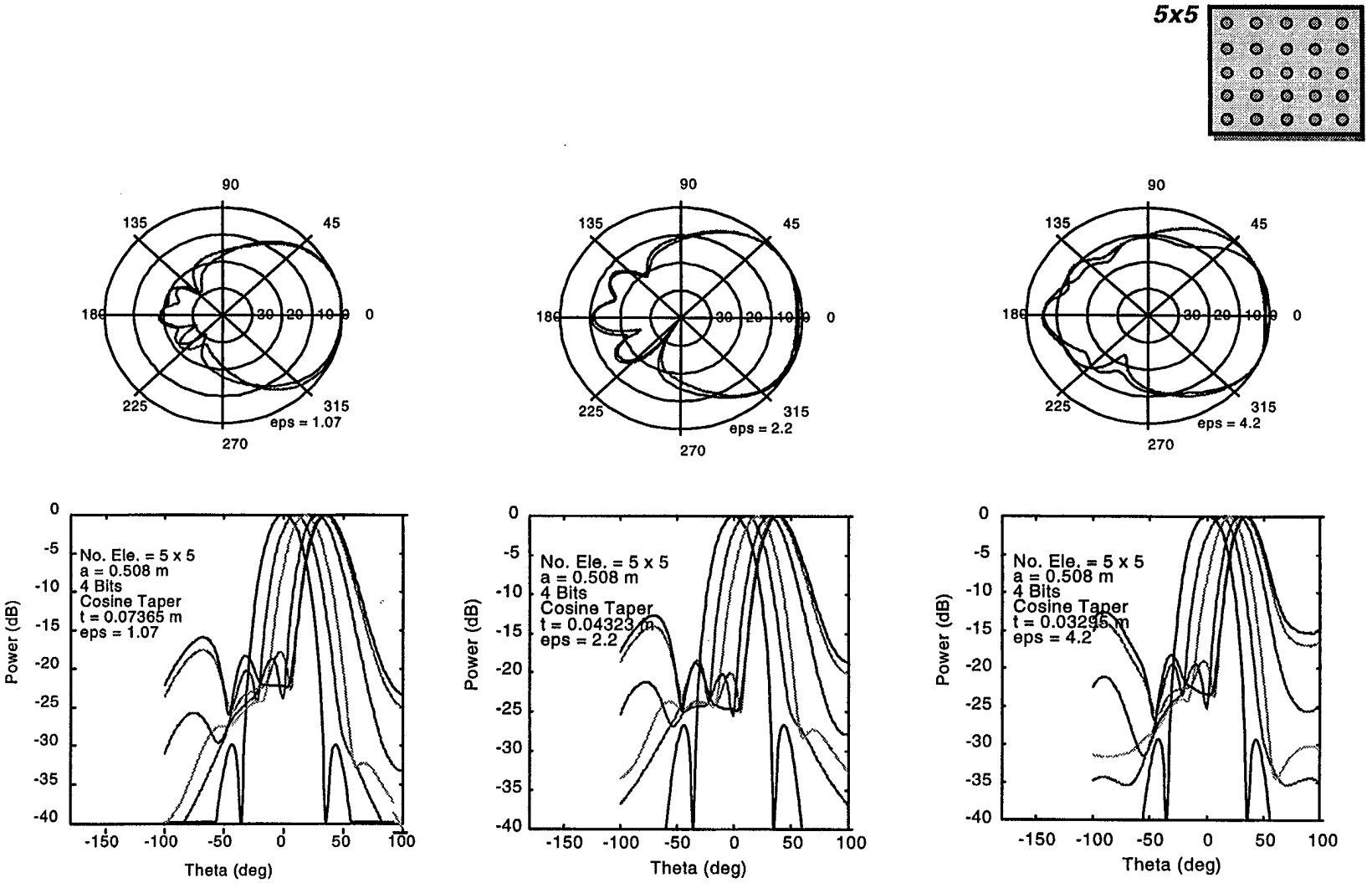

Figure 5. Steering UHF array of circular patches.

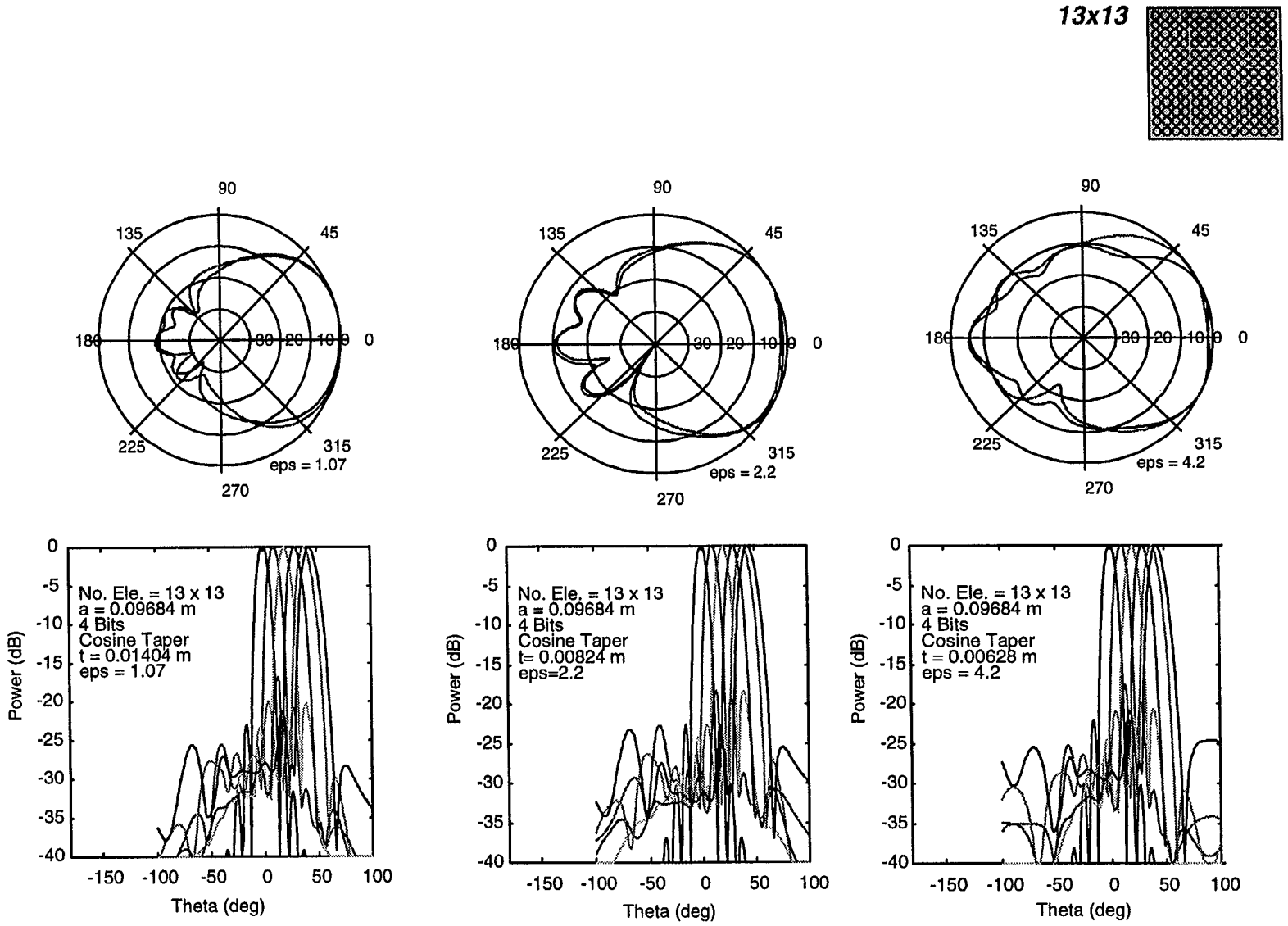

Figure 6. Steering INMARSAT array of circular patches.

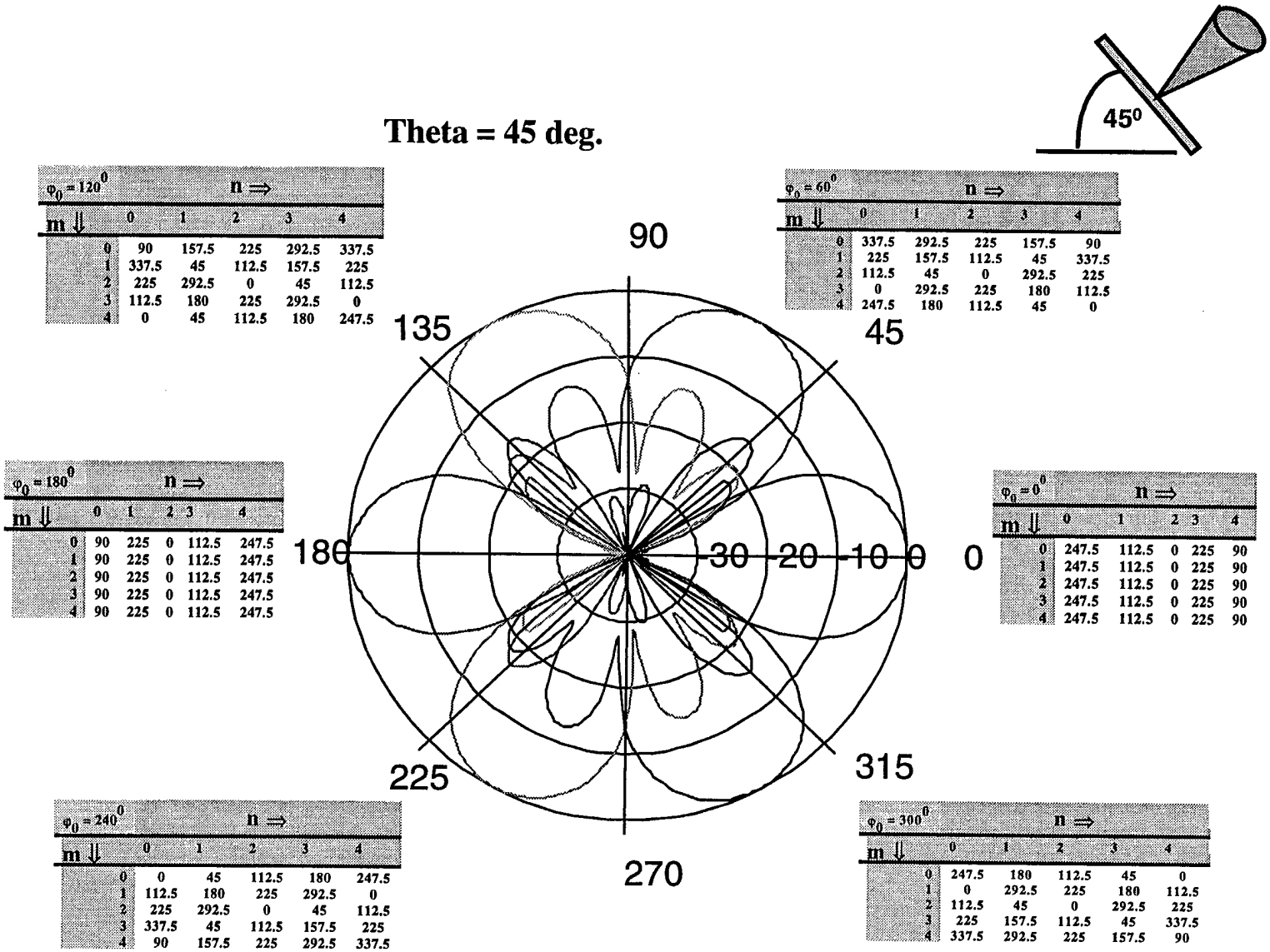

$\varphi_0 = 120^0$ — n ⇒

m ⇓	0	1	2	3	4
0	90	157.5	225	292.5	337.5
1	337.5	45	112.5	157.5	225
2	225	292.5	0	45	112.5
3	112.5	180	225	292.5	0
4	0	45	112.5	180	247.5

$\varphi_0 = 60^0$ — n ⇒

m ⇓	0	1	2	3	4
0	337.5	292.5	225	157.5	90
1	225	157.5	112.5	45	337.5
2	112.5	45	0	292.5	225
3	0	292.5	225	180	112.5
4	247.5	180	112.5	45	0

$\varphi_0 = 180^0$ — n ⇒

m ⇓	0	1	2	3	4
0	90	225	0	112.5	247.5
1	90	225	0	112.5	247.5
2	90	225	0	112.5	247.5
3	90	225	0	112.5	247.5
4	90	225	0	112.5	247.5

$\varphi_0 = 0^0$ — n ⇒

m ⇓	0	1	2	3	4
0	247.5	112.5	0	225	90
1	247.5	112.5	0	225	90
2	247.5	112.5	0	225	90
3	247.5	112.5	0	225	90
4	247.5	112.5	0	225	90

$\varphi_0 = 240^0$ — n ⇒

m ⇓	0	1	2	3	4
0	0	45	112.5	180	247.5
1	112.5	180	225	292.5	0
2	225	292.5	0	45	112.5
3	337.5	45	112.5	157.5	225
4	90	157.5	225	292.5	337.5

$\varphi_0 = 300^0$ — n ⇒

m ⇓	0	1	2	3	4
0	247.5	180	112.5	45	0
1	0	292.5	225	180	112.5
2	112.5	45	0	292.5	225
3	225	157.5	112.5	45	337.5
4	337.5	292.5	225	157.5	90

Figure 7. Conical scan with UHF array.

As we discussed earlier, there are many methods that one can use to combine the simultaneous antenna beams. In this study we outlined two different approaches. In either case, the signal distribution network is the key factor in achieving simultaneous beams. One of the technology areas critical to this future development is multiplexing technology. This device will allow the signals to combine or separate depending on the actual applications. Recent development of this technology has focused on the miniaturization of such devices. Figure 8 shows some results. The left-hand side of the figure shows the diplexer (2) that can be utilized for INMARSAT application. It is low-profile in packaging density and conformal so that it can be integrated along with the antenna panel. The performance of the diplexer is also shown on the right with insertion loss (attenuation) as a function of frequency. An isolation of >50 dB between transmit and receive can be achieved with this technology. The typical insertion loss of the passband is 0.35 db.

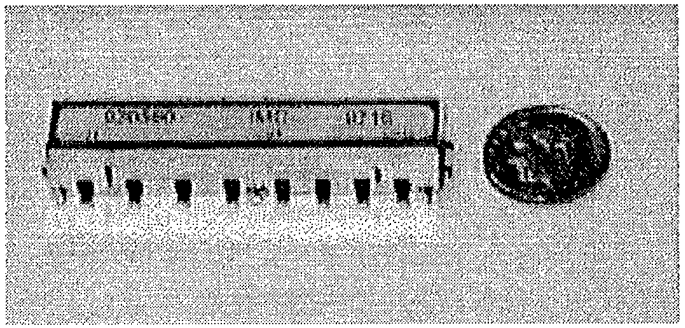

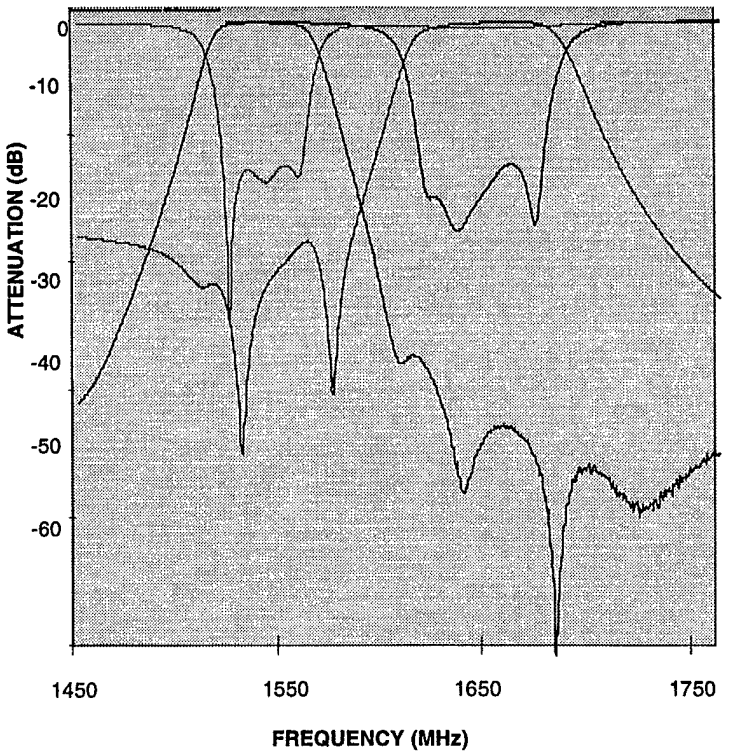

Figure 8. INMARSAT diplexer.

7. CONCLUSIONS AND RECOMMENDATIONS

The results of the above section demonstrate that either square or circular patches, when used in an array, can perform the UHF and INMARSAT functions. The phased-array antenna technology can be utilized in place of a legacy mechanical steering system. The advantages of the new technology may include enhancing system performance, improving reliability due to less-exposed environment and making the antenna less vulnerable to hostile detection. Signature control is the driving criteria in many of the future surface combatant designs.

Our preliminary study indicates that a dual-frequency system (four beams) could be developed with 25 patches designed to the UHF band and 169 designed to the L-band. Further study is needed to determine the impact of the crossover on antenna performance when the beam is steered azimuthally. Additionally, new technology options for multiplexing need to be developed so that they can be implemented at high frequencies with minimum profile. Future study may also include the validation of our first antenna concept. Although this is the most aggressive approach, it has many benefits including requiring a single antenna set and a single-signal distribution network for simultaneous beam operations.

8. REFERENCES

Elliott, R. S. 1981. *Antenna Theory and Design.* Prentice-Hall, Inc. New York, NY.

Hall, P. S. 1995. "Review of Techniques for Dual and Circularly Polarized Microstrip Antennas," In *Microstrip Antennas, The Analysis and Design of Microstrip Antennas and Arrays*, IEEE Press. New York, NY.

Ho, T. Q. 1994a." An Experimental Bandpass Frequency Selective Surface Radome." NRaD* Technical Document 2611. Space and Naval Warfare Systems Center, San Diego, CA.

Ho, T. Q. 1994b." Development of an Integrated FSS Antenna." NRaD Technical Document 2716, Space and Naval Warfare Systems Center, San Diego, CA.

Kishk, A. A. and Lotfollah Shaffai. 1986. "The Effect of Various Parameters of Circular Microstrip Antennas on Their Radiation Efficiency and the Mode Excitation," *IEEE Transactions on Antennas and Propagation* (Aug), vol. AP-34, no. 8, pp. 969-976.

Maxwell Eminence, Version 4.0, 1995.

Munson, R. E. 1974."Conformal Microstrip Antennas and Microstrip Phased Arrays," *IEEE Transactions on Antennas and Propagation* (Jan), p. 74.

Space and Naval Warfare Systems Command. 1991. "Navy UHF Satellite Communication System Description," FSCS-200-83-1(31 Dec).

---

* Now Space and Naval Warfare (SPAWAR) Systems Center, San Diego.

TASK 2
LOS ANTENNA CONCEPTS AND ELECTRONICS IN SUPPORT OF THE MERS ATD

This task was divided into two subtasks. The objective of the first subtask was to conduct a preliminary study of developing a one-dimensional, phased-array antenna for Joint Tactical Information System (JTIDS) applications. The focus of the second subtask was to develop novel high-power electronics, specifically, UHF circulators and frequency-hopping filters, to support the MERS ATD technology options.

SUBTASK 1
DIRECTIONAL ANTENNA CONCEPT FOR JTIDS APPLICATIONS

1. INTRODUCTION

The current Joint Tactical Information Data System (JTIDS) antenna is an array of 16 pairs of dipoles arranged around a 3-foot-diameter cylinder. The latest version is enclosed in a frequency-selective radome with tilted sides. The JTIDS antenna is designed to have a pattern that is omni-directional in the horizontal plane. The frequency range is 960 to 1215 MHz. The development of a version of JTIDS with a directional capability is desirable due to more stringent operational requirements (e.g., Link 16). Such an antenna concept would allow terminals to communicate at greater range; therefore, it would enhance the current JTIDS processing capabilities.

2. CONCEPTUAL DESIGN

The requirement to reduce the radar cross section (RCS) of antennas located on the topside of surface combatants imposes severe restrictions upon antenna design. Generally, legacy antenna systems do not provide signature control. This is a major concern to many combatant designers. Future surface combatants emphasize low signature profile to meet operational requirements in a hostile environment. Our approach to a directional JTIDS is to apply phased-array antenna technology. This approach will allow elements to be embedded inside the superstructure while steering the antenna without mechanically moving parts. Design considerations also include both the shape of the antenna element and supporting superstructure and the use of frequency-selective surfaces. Figure 9 presents a summary study of the RCS profile for a superstructure of varying shapes. The primary differences between these models are the number of sides (conical, hexagonal, or octagonal), the tilt angle of the sides from the zenith, and a 20° tilted structure that is treated with radar absorbing material. The horizontal line denotes the preliminary requirement for combatants in the 21st century.

This study indicates that the hexagonal, untreated structure is far better for RCS than either the conical or octagonal structure. In general, the RCS reduces as the tilt angle increases. This is due to less penetrating energy coming back to the original source. Only for large tilt angles does the octagonal structure meet the requirement. Treating the sides of the superstructure with radar-absorbing material is very expensive. Additionally, this methodology may create an infrared (IR) problem. Due to the many advantages that the hexagon has for RCS, the Multifunction Electromagnetic Radiating System (MERS) is adapting this baseline. Our study for the directional JTIDS antenna follows the MERS guidelines.

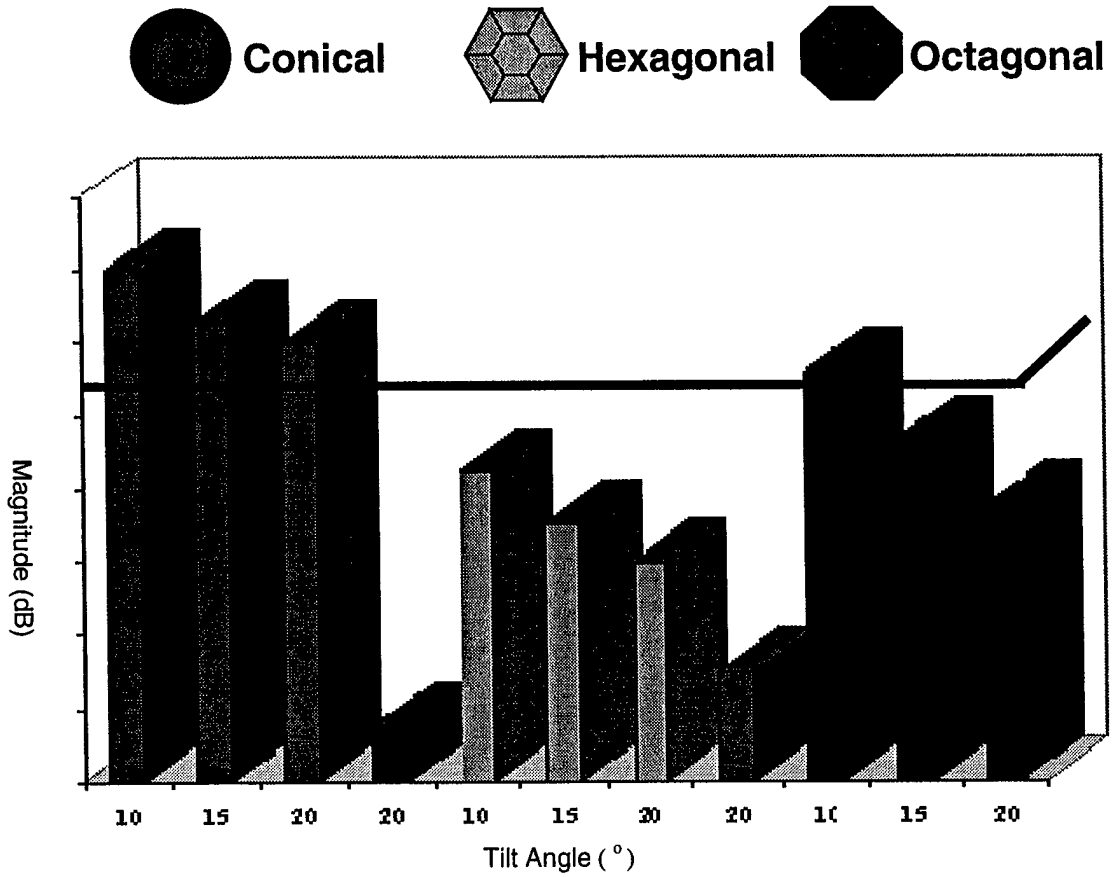

Figure 9. Signature shaping options.

3. NUMERICAL RESULTS

In this study we selected conformal bowties as the antenna elements for JTIDS. Conformal bowties are more suitable in this application than the conventional dipoles due to their high bandwidth characteristics. This is one choice of the antenna elements. Other types of elements should also be considered. Various analytical antenna codes were used to study numerous design options for directional JTIDS. After Maxwell Eminence was used to generate the fields of one element, array theory was utilized to generate the fields of many configurations. Figure 10 shows various design options for directional JTIDS. Six different cases were investigated in an effort to reduce the array's diameter. The elements were arranged in one row around a conical structure with a 20° tilt angle. Their locations were such that 64 could be distributed around the base of the cone. The number of active elements was 16, 24, or 32 at any given time. The two distribution networks used in this study were cosine and modified cosine tapers. The amplitude distribution options are shown on the right. The beamwidth of the directional beam as a function of diameter of the array is shown on the left. The two horizontal markers represent the desired beamwidth for JTIDS operation. Typically, the larger the diameter of the array, the smaller the antenna beamwidth. The amplitude distribution of power to the elements in the array also has a significant effect upon such properties as the beamwidth and side lobe level. This figure presents the results for the beamwidth as a function of the array diameter, the number of elements activated, and the amplitude distribution. In general, the more elements used and the more uniform the taper, the smaller the beamwidth for a given diameter of the array. However, these conditions also cause the side lobe level to increase.

Figures 11 and 12 present the radiation patterns for the six design options (three numbers of elements and two tapers). These are the radiation patterns for an array with the particular diameter that causes the beamwidth to be 8° and 10°, respectively. The side lobe level is typically less than 30 dB, with very low spurious response. The larger the numbers of elements used, the smaller the diameter must be to achieve a particular beamwidth.

Our next step was to investigate the performance of the antenna when the array was no longer conical. The motivation behind this study was due to the newly defined platform for the future combatants. Combatant designers are seriously considering hexagonal or octagonal over conical topsides due to considerations of the RCS issue. The objective of this study was to understand the impact of panel junctions on antenna radiation characteristics when phased-array technology is applicable. Almost no information on such phenomena is now available. We started our study with an octagonal structure. In this configuration, the phased-array antenna elements are distributed equally among eight different faces. There were eight elements per face and 24 are active at any given time. The diameter of the octagon was taken as the distance between opposite faces.

Figure 13 shows some of the results that we have so far. The figure on the left indicates the amplitude distributions used in the study. In the first, the maximum amplitude was at the center of the face (90°). For the second, the maximum was near the junction between faces (112.5°). Array theory was then used to examine the beamwidth characteristic of the antenna as a function of the array diameter. The preliminary data indicated that the location of the main antenna beam has little effect upon the beamwidth. Table 4 data also support this conclusion. This table shows the antenna main lobe beamwidth varying across the panel junction as a function of tilt angle. The tilt angle varied

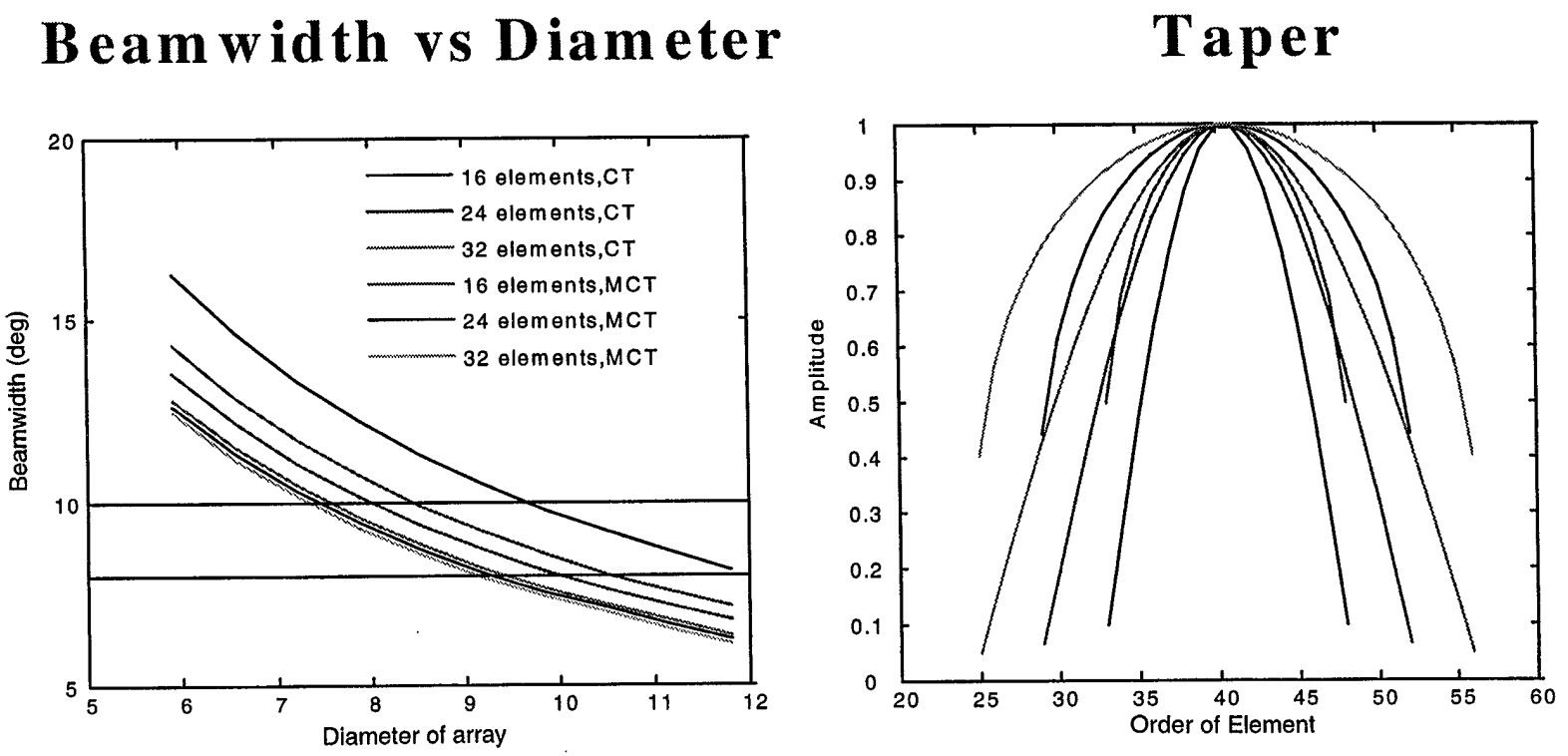

Figure 10. Conical array of bowties.

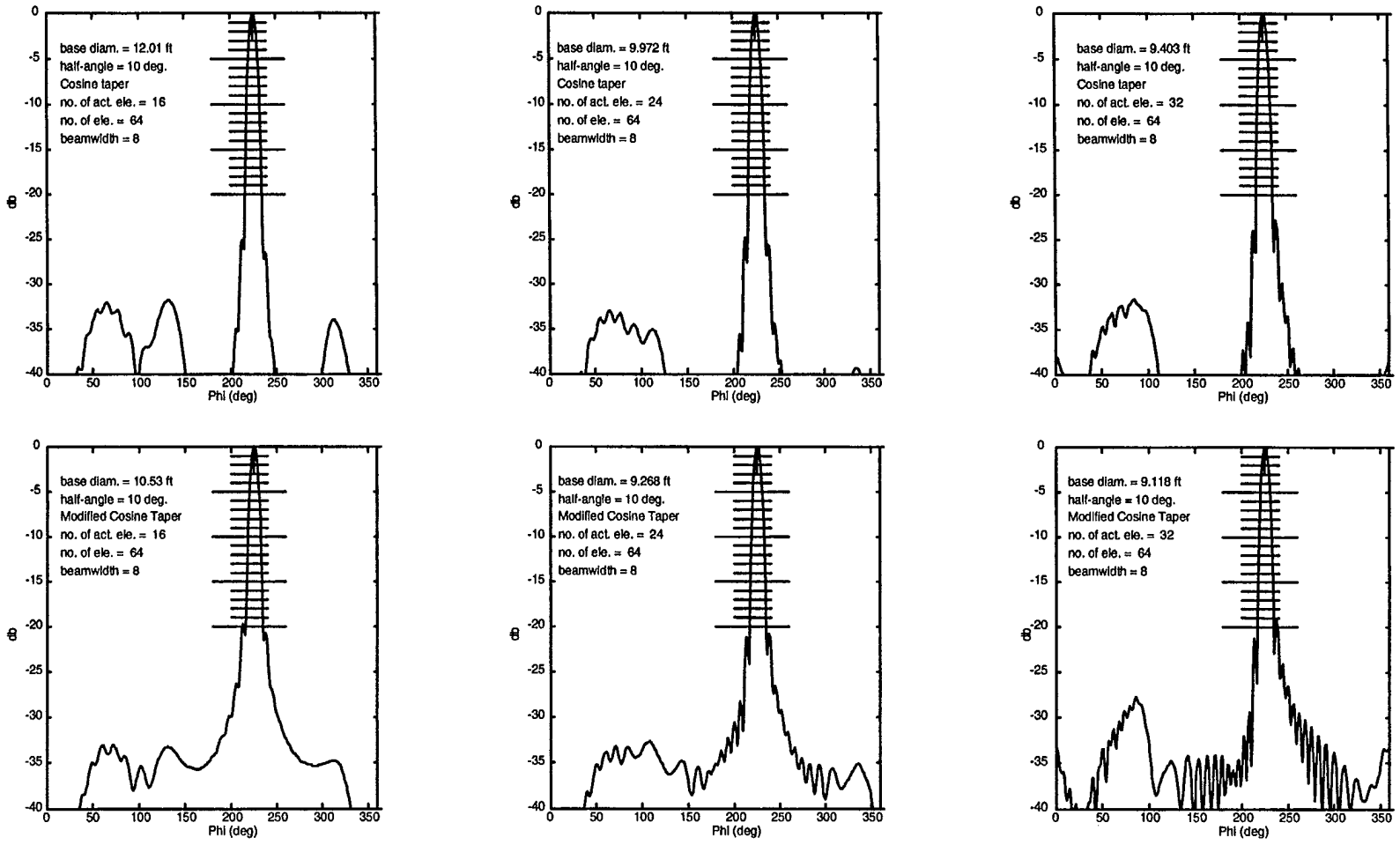

Figure 11. Radiation patterns of 8° beamwidth arrays.

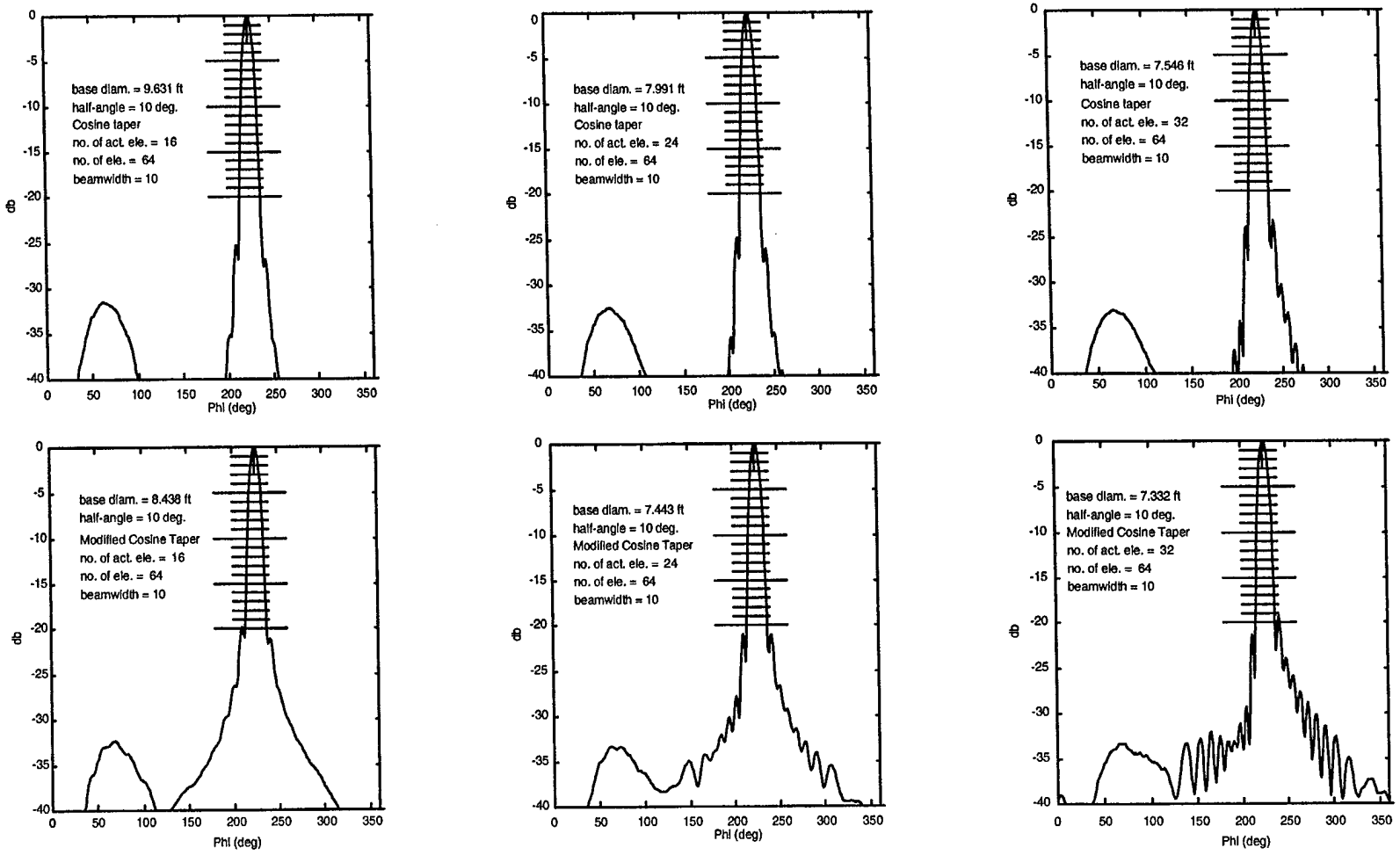

Figure 12. Radiation patterns of 10° beamwidth arrays.

Taper

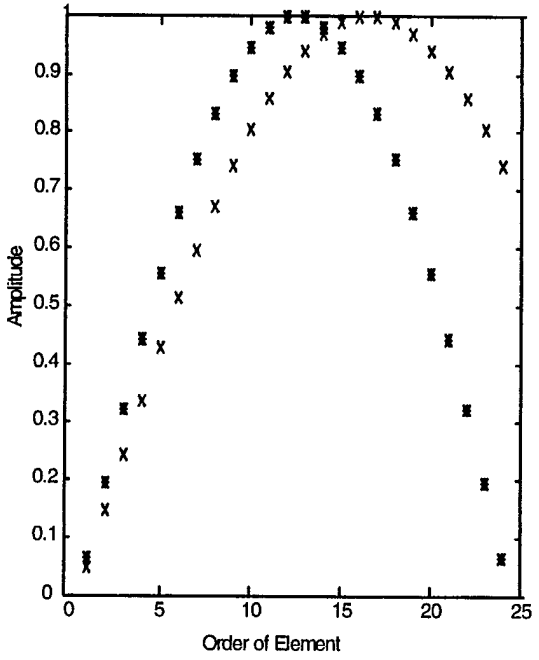

Beamwidth vs Diameter

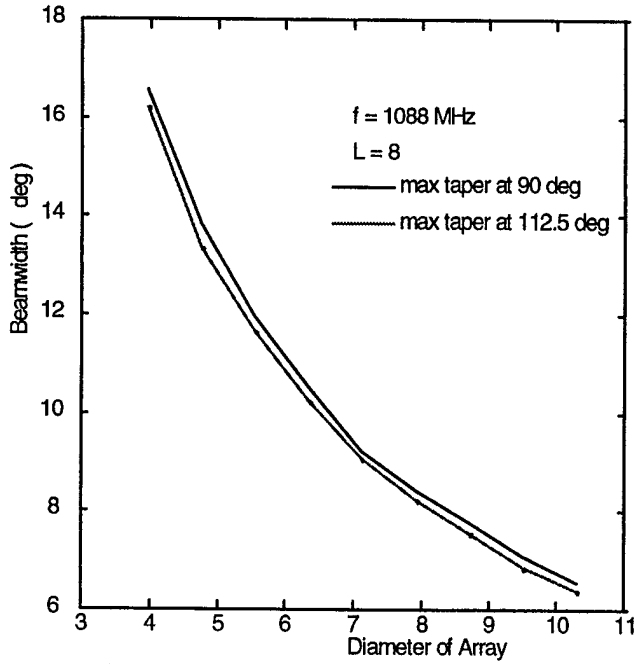

Figure 13. Octagonal array at L-band.

from 10° to 45°. The data show that tilting the beam has a much greater effect on the antenna beamwidth. Typically, the beamwidth increases with increasing tilt angle.

Table 4. Beamwidth distortion of the L-band array.

$\phi(e_{max})$	$\gamma = 10$	$\gamma = 20$	$\gamma = 30$	$\gamma = 45$
110.13	8.1186	8.1777	8.6007	9.7387
11.45	8.1240	8.2274	8.5748	9.7676.
110.91	8.1257	8.2553	8.6471	9.7456
111.20	8.1344	8.2482	8.6591	9.7895
111.52	8.1521	8.2780	8.6125	9.8690
111.96	8.1476	8.2843	8.6471	9.8067
112.22	8.1346	8.2519	8.6841	9.7715
112.56	8.1977	8.2762	8.7011	9.8638
113.07	8.1283	8.2919	8.7134	9.9129
113.34	8.1658	8.3067	8.7080	9.8668
113.64	8.1837	8.2586	8.7296	10.0731
114.04	8.1966	8.2886	8.7686	9.9229
114.34	8.2027	8.3043	8.7759	9.8246
114.59	8.1872	8.3165	8.7621	9.9251
115.05	8.2091	8.3174	8.7679	10.0020
115.53	8.2194	8.3257	8.7938	9.9752
115.79	8.2392	8.333	8.8269	10.0250

These results show that tilting the array, encouraged by the need to reduce RCS, has a significant effect upon the beamwidth. The use of large numbers of elements in a cylindrical or octagonal array with a 7.5-foot diameter can reduce the beamwidth to less than 10°.

4. CONCLUSIONS AND RECOMMENDATIONS

This study indicates that conformal phased-array antenna technology can be used to design the directional antenna requirements for JTIDS applications. Various design options were considered along with the predicted performance. These options included a 64-element baseline. The beam can be steered using 4-bit phase shifters. Further study is necessary to determine the full impact of the junctions on antenna performance when the beam is steered azimuthally, especially for four-sided or six-sided structures. Additionally, software design tools and methodologies for designing nonconformal phased-array antennas need development to accommodate future combatant platforms.

SUBTASK 2
NOVEL ELECTRONICS FOR UHF APPLICATIONS

1. INTRODUCTION

Future surface combatants (e.g., SC21, Arsenal Ship, CVX) will have to meet stringent operational requirements (e.g., RCS, C4I Link Availability) for anticipated missions such as the littoral one. Major technical challenges associated with increasing antenna system performance and functionality while concurrently reducing antenna system Radar Cross Section (RCS), electromagnetic interference (EMI), volume, and weight must be addressed to achieve these goals. The principal objective task is to develop technology options that will enable design, development, and demonstration of affordable multifunctional antenna system concepts in support of future ships.

Single-service shipboard antenna systems currently minimize EMI with one another by maximizing their physical separation. The physical separation between antennas must be minimized to enable antenna systems to be multifunctional. As antenna systems are consolidated, the isolation required between them to mitigate EMI must now be achieved in the signal distribution network that excites them. This EMI problem necessitates the development of advanced electronic components for high-power isolation networks including wideband-shared radio frequency (RF) amplifiers, cancellation circuits, high-power circulators, and frequency-agile filters/multiplexers. The synergistic effect of this electronics technology is the ability to achieve isolation between consolidated antenna systems in a densely packaged volume. The Office of Naval Research's (ONR) Multifunction Electromagnetic Radiating System (MERS) Advanced Technology Demonstration (ATD), which will eventually incorporate SLICE Radio (30 MHz to 2 GHz) and transition to JMCOMS, serves as a real example of antenna consolidation.

2. TECHNICAL OBJECTIVES

The most challenging communications systems to consolidate into a single aperture are the UHF radios. On the DDG 51 class ships, there are currently 18 UHF Line-of-Sight (LOS) radios. These radios are distributed in the following manner: two URC-93 (V)1 and (V)2 radios; 14 WSC-3 (V)7 radios; and two WSC-3 (V)11 radios. The URC-93 radios can operate in the full-duplex mode of operation and the WSC-3 (V)11 radios can operate in the frequency-hopping (antijam) mode of operation. The MERS UHF architecture must incorporate full-duplex and antijam modes of operation.

Figure 14 shows the UHF electronics architecture that can consolidate multiple antijam, full-duplex radios into a single antenna structure. Starting from the transmit path, the radios will be modified so that control and RF signals will be transmitted through fiber-optical links from the Radio Room, up the mast, and into the MERS antenna structure. Within the MERS antenna structure, the RF signals will be amplified to 30 watts maximum average power per channel in the LOS mode and 100 watts maximum average power per channel in the SATCOM modes and FM LOS modes. Next, the control signals will tune each filter to the frequency corresponding to the radio channel. This is done within the signal combiner stage of the architecture. Finally, the combined and amplified RF signals are transmitted through the circulator and diplexer to the antenna structure where it is radiated. For the receive path, the reverse chain of events occurs to complete the link.

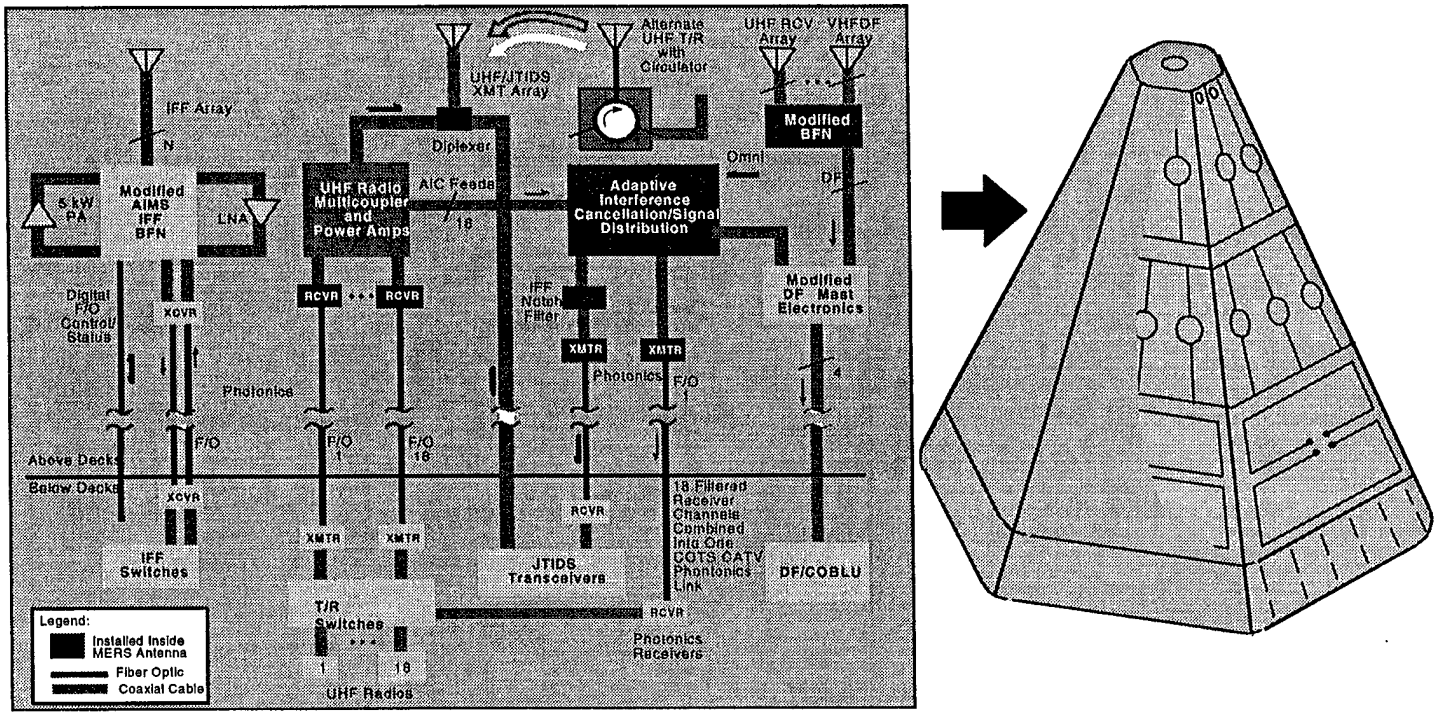

Figure 14. MERS ATD concept.

3. TECHNICAL APPROACH

For multifunctional antenna concepts such as the MERS ATD (figure 14) to incorporate full-duplex antijam capabilities successfully, novel electronic components such as the wideband high-power circulators and frequency-hopping filters need to be developed and demonstrated as a viable option. As shown in table 5, preliminary UHF system requirements were developed to provide baseline system specifications for the planned UHF electronics architecture.

Table 5. UHF requirements.

Frequency	225 to 400 MHz
No. of carriers	18
No. of channels	7000
Channel spacing	25 kHz
Preset channels	20
Tx power	100 W/channel FM, PSK, FSK
	30 W/ channel AM
Rx selectivity	+/-15 kHz, minimum, 3 dB
	+/-50 kHz, maximum, 60 dB
Spurious radiation	-50 dB within 5 MHz of carrier
	-80 dB within 5 to 20 MHz of carrier
	-100 dB greater than 20 MHz from carrier
Harmonics	60 dBc
Noise Figure	8 dB
Isolation	60 dB

4. TECHNICAL RESULTS

4.1 DISTRIBUTED ELEMENT CIRCULATOR

During FY 97, the state-of-the-art 1-kW UHF octave bandwidth circulator was developed using a distributed element approach. Figure 15 shows this circulator. The prototype has a diameter of 7.9 inches and weighs approximately 14 pounds. The prototype was built in hybrid form so that modifications could be readily implemented to achieve the optimal circulator performance. The matching elements are in a stripline form so that dissipation and insertion losses are minimized. The magnetic disks are mounted inside a reduced waveguide junction to reduce the circuit footprint.

The AFT CVG7 material with a 1762 $4\pi Ms$ was selected for this experimental study. We used an iterative process to determine the ideal parameters. Initially, the disk parameters of R = 0.500 inch and T = 0.100 inch were selected for the ferrite hexagon. R represents the larger radius of the hexagon and T is the thickness of the ferrite slab. The measured response proved to be too low in operational frequency and too narrow in bandwidth to meet the goal of operating between 225 to 400 MHz. Our first step was to allow redesign to optimize dimensions. The ferrite was then re-built to a dimension of R = 0.333 inch and T = 0.075 inch with the corresponding matching transformers for the smaller ferrite geometry. Figure 16 shows the results of this second model. The prototype showed an insertion loss of less than 0.9 dB and a typical return loss of 13.0 dB over the frequency band of 180 to 333 MHz (60% bandwidth). After an extensive tradeoff study, the ferrite hexagon at the junction was further reduced to R = 0.313" for an operation from 225 to 400 MHz. In this case, the higher order resonance mode was pushed above 400 MHz to obtain a flat, continuous bandpass within the frequency range. The high order mode was also partially reduced by placing 0.025-inch-thick brass between the ferrite and steel magnetic ground planes to damp out the radiation.

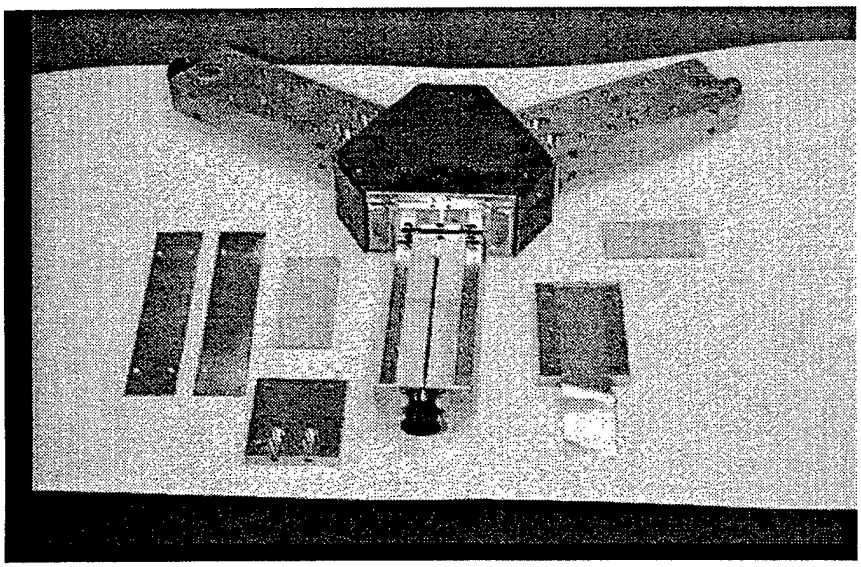

Figure 15. 1-kW UHF circulator.

The stripline transformer sections were designed using D16 ($e_r = 16$) and DA9 ($e_r = 9.5$) dielectrics. The ceramic dielectric blocks forming the quarter-wavelength sections, which were physically longer than required, resulted in transformer sections electrically longer than a quarter-wavelength. To compensate, a small section of the circuit at the input of the first transformer was reduced in width to provide a small amount of compensating inductance. This optimized the return loss, insertion loss, and isolation. Inductive compensation will not be necessary in the final product design. Both dielectric blocks were completely shielded from the housing to effectively isolate the circuit from parasitic effects. The width of the distributed transformers in the final iteration was reduced by 0.008 inch from the previous iteration to properly match junction-input impedance.

Figure 17 shows the performance of the state-of-the-art circulator. The insertion loss was less than 0.5 dB, and isolation was typically 15 dB or better across the frequency band (from 225 to 400 MHz). This measurement was conducted under low-power conditions using a HP network analyzer. Figures 18 and 19, respectively, show high-power measurements for insertion loss and isolation. The insertion loss typically increased by 0.25 dB from a low-power level to 1-kW. This could be defined as a ¼ dB compression point. The isolation profile seemed to be the same at the high-power level, except for the low-frequency end. Typically, an isolation of 15 dB is achievable. Since our measurement capability for the high-power signal generator was limited to 1-kW, the 1-dB compression point could not be reached and determined. The circuit was tested for the intermodulation distortion products. Two-toned signals at ¼ of the rated power were injected into the device under test to determine the third-order interception point. A level for an IP3 of 85 dBm was obtained at 1 kW with the new circulator. The IP3 number suggested that the device was still operating in the linear range even at this power level. In actuality, this phenomenon can be observed through the 1-db compression study.

4.2 HIGH-POWER FREQUENCY-AGILE FILTERS

4.2.1 Design Considerations

In FY 96, a 4:1 frequency-agile combiner (<20 W) was demonstrated across the UHF band (2:1) from 225 to 400 MHz. To incorporate planned future upgrades to MERS, this electronic component must operate across the entire band at a much higher power level. The key element in this development is the frequency-hopping filter. In FY 97, the objective was to develop a viable filter option that will enable design, development, and demonstration of affordable multifunctional antenna system concepts in support of future ships.

The preliminary requirements are: 1) power rating @ 100 W; 2) bandwidth of 2%; 3) frequency of operation from 225 to 400 MHz, and 4) insertion loss of < 1 dB. Figure 20 illustrates the filter concept. The values of capacitance that determined the filter's operational frequency could be chosen from among 14 standard values. The PIN diodes serve as ON/OFF switches to allow determination of the effective capacitance value.

The development of this technology for high-power applications involves tradeoffs due to many limitations. These issues are primarily due to the imperfect nature of the actual circuit, specifically, voltage breakdown and power dissipation. These relationships between current, voltage, and power are given by $P = V^2/R$ and $P = I^2R$. Given the assumption that the components are not thermally limited, the circuit will eventually reach the breakdown voltages at some power level. This effect is

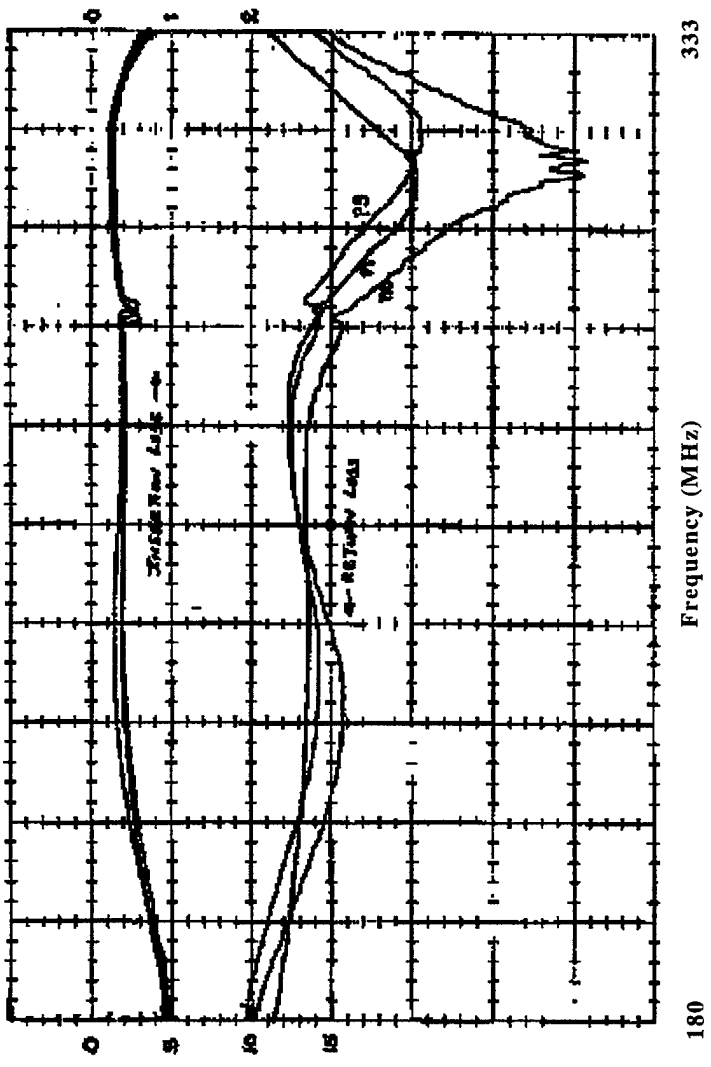

Figure 16. Circulator performance from 180 to 333 MHz.

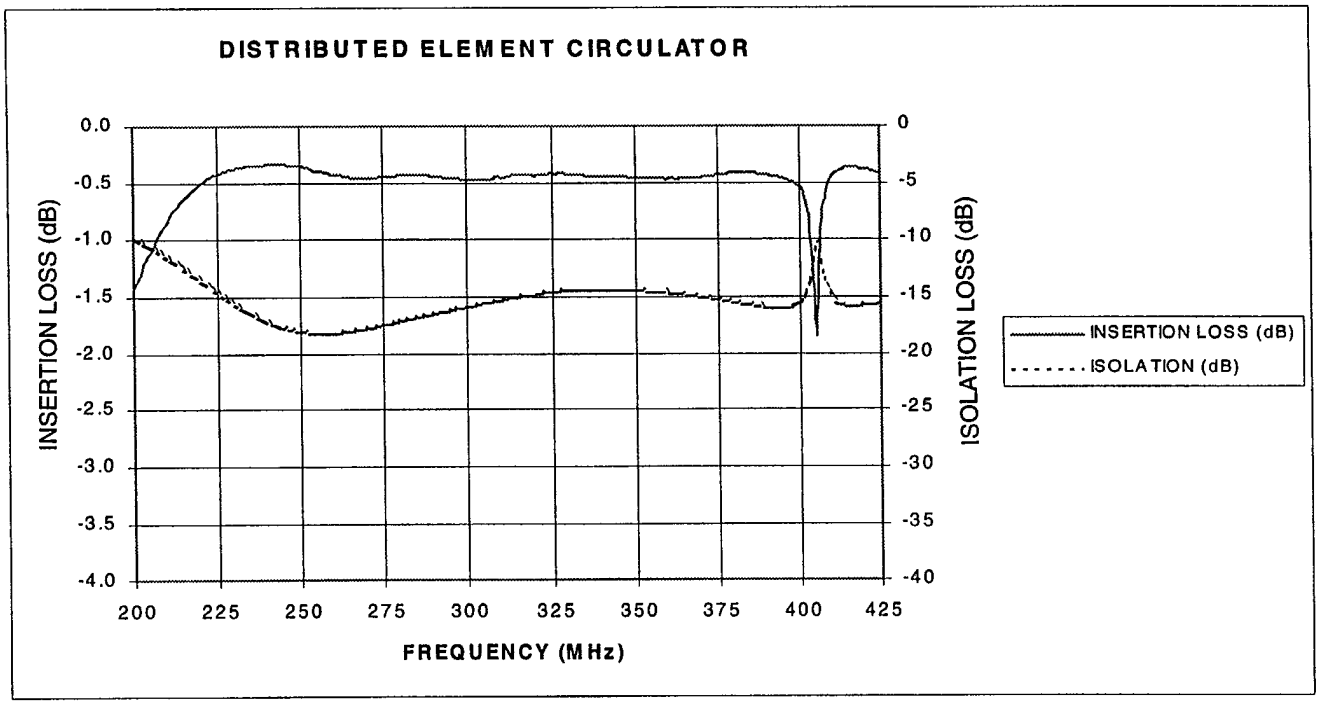

Figure 17. Circulator performance from 225 to 400 MHz.

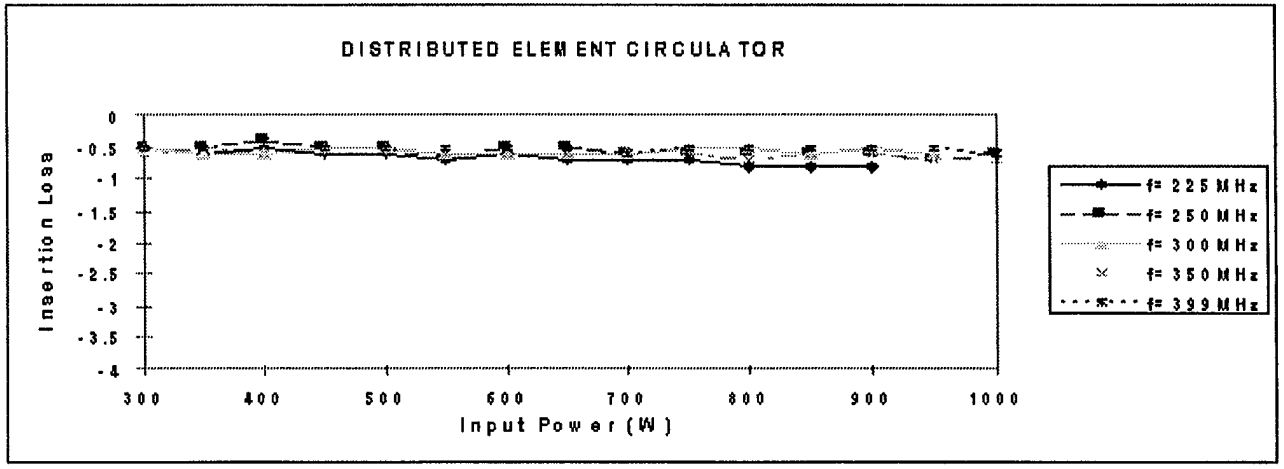

Figure 18. Insertion loss versus input power.

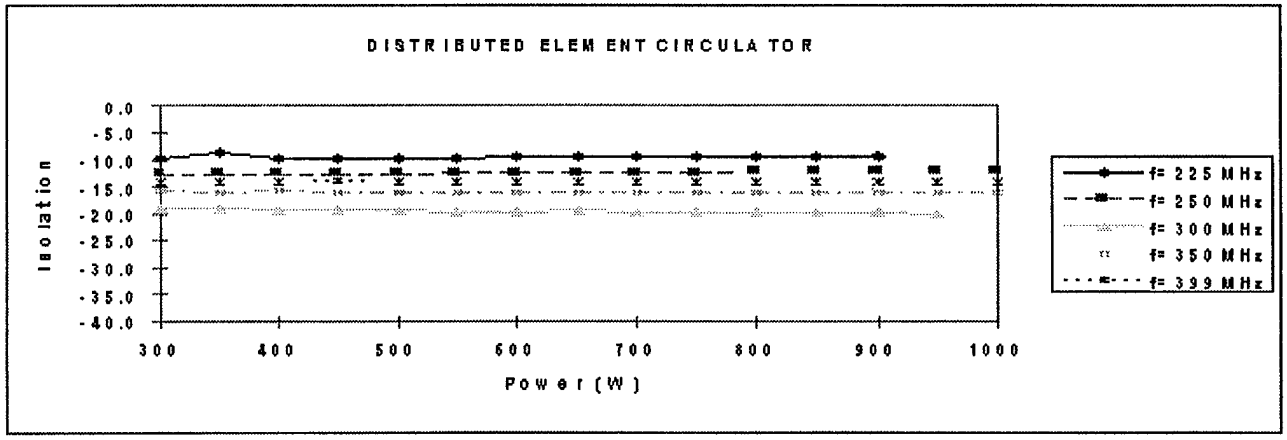

Figure 19. Isolation versus input power

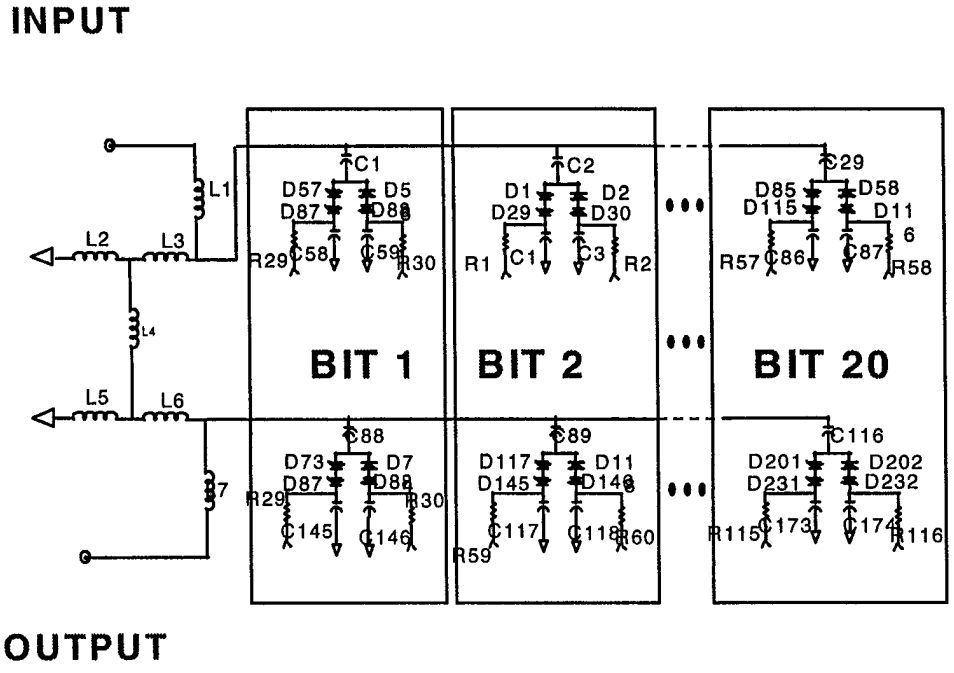

Figure 20. Circuit topology for 100-watt UHF frequency-hopping filter.

compounded in a band-pass filter due to high Q cavity that is frequently used in the design to achieve sufficient out-of-band rejection. Filters are designed to have the impedance of the resonator fall within the frequency range. Since the Q of a resonant circuit is related to the impedance by the relationship, $Q = R_p/X_p$, where R_p is the effective parallel resistance and X_p is the reactance of either of the reactive elements, the parallel resistance of the circuit is directly related to the Q of the circuit. A higher Q factor, which is a measurement of selectivity, also increases the filter voltages. This unavoidable phenomenon is one of the primary limiting factors in the design of very-high-power filters.

The circuit elements that first reach their voltage limits are the capacitor and the PIN diode. Commercial capacitors suitable for UHF filter design are often referred to as "B-chips" and "E-chips." Their main difference is size and, consequently, power and voltage handling. The larger size capacitors are not currently produced with the highest Q materials. It is probable that manufacturers could improve the capacitor Q up to four-fold. The smaller package is a cube with a volume of 0.001 cubic inches, lending itself to a compact, low-parasitic layout at UHF frequencies.

The second limiting factor is the PIN diode used for switching the bit gap into the circuit. Although commercial diodes are available up to breakdown voltages of 3000 Vbr, these devices are not effective due to poor isolation between ON and OFF states. The "on" resistance and "off" capacitance are both too large to be practical, especially at this frequency. Therefore, the model under development is based on either a 100 Vbr or 1000 Vbr diode. By considering the maximuum tank voltage, the required selectivity, and the resonator, Xp, the maximum possible power level can be computed. The calculation of the voltage-derived power handling described above assumes an ideal load.

The second issue that must be addressed is the filter power dissipation. The attributes are from the DC and RF components. The DC component may include the PIN diode and H.V. bias switching dissipations.

Table 6 lists our estimated DC power sources for this high-power filter.

Table 6. Estimated DC power sources for high-power filter.

Description	Supply	Power
Forward-diode bias	-5 Vdc @ 24A Max	120 W
Logic control	+5 Vdc @ 1A Max	5 W

In general, the current consumption changes with hopping rate and filter tune position. The forward-bias diode current increases when the filter is tuned towards the lower end of the spectrum. The highest forward-bias diode occurs at 225 MHz when all the PIN diodes are forward-biased. The H.V. bias supply current also changes. This supply current is dependent on hopping rate and filter tune position. The preliminary data show that the energy required to switch these components from one state to another is approximately 106 uJ. This number translates into a corresponding worst-case

total heat dissipation in this filter of 52 W. Although theoretical, this value gives an insight into whether this newly developed filter can handle an input power level of 100 W continuous wave (CW).

4.2.2 Experimental Results

Figure 21 shows the state-of-the-art 100 W CW frequency-agile filter. Although this filter presently switches between only two frequencies, these data suggest that a frequency-hopping filter that meets UHF requirements is possible. The inductors are realized using cavities. The high Q cavity is approximately 6 x 3 x 2.5 inches and weighs 0.1 pound. This is a significant reduction in size and weight compared to the current tunable filter used in multicouplers (Model OA-9123/SRC). The current tunable filter cannot be used in frequency-hopping systems. A 20-bit PIN-diode switching architecture capacitively tunes the two-section filters between the desired frequencies of the operation.

Figure 22 shows the data of the same high-power filter tuned between 233.75 MHz and 399.69 MHz. The insertion loss was measured to be 2.4 dB at the low end and 2.1 at the high end of the band. This loss included all PIN-diode switches and connectors. The return loss was measured to be 16 dB and 20 dB, respectively, at lower and higher ends of the frequency spectrum. The percent bandwidth, defined as the ratio of the 3-dB bandwidth to the center frequency, was typically 1.6%. The shape factor, defined as the ratio of the 30-dB bandwidth to the 3-dB bandwidth, was typically 7. The harmonics are better than 110 dBc and the 1-dB compression point is exceeded 100 watts. The third order intercept point was 75 dBm.

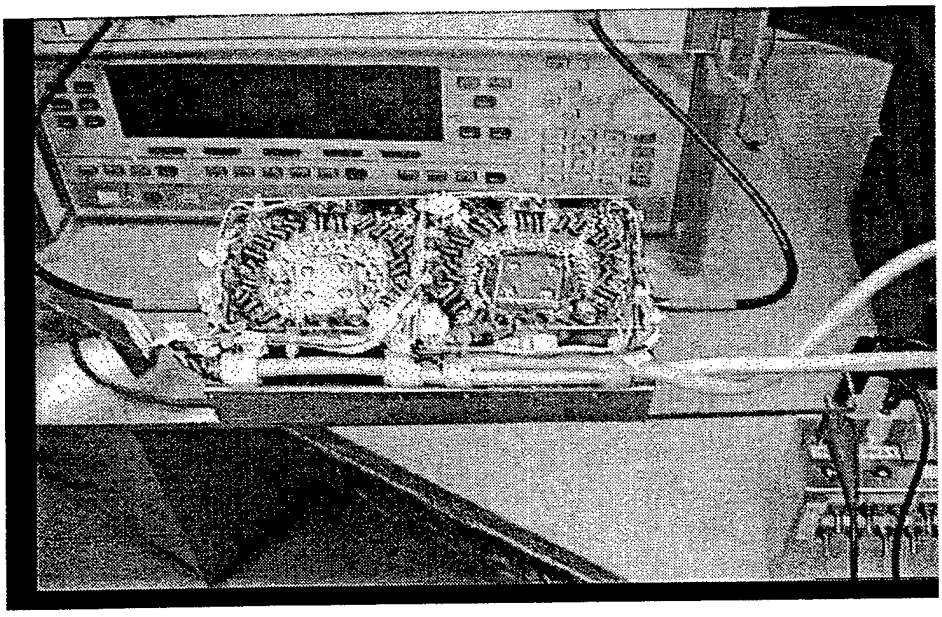

Figure 21. 100-watt frequency-hopping filter.

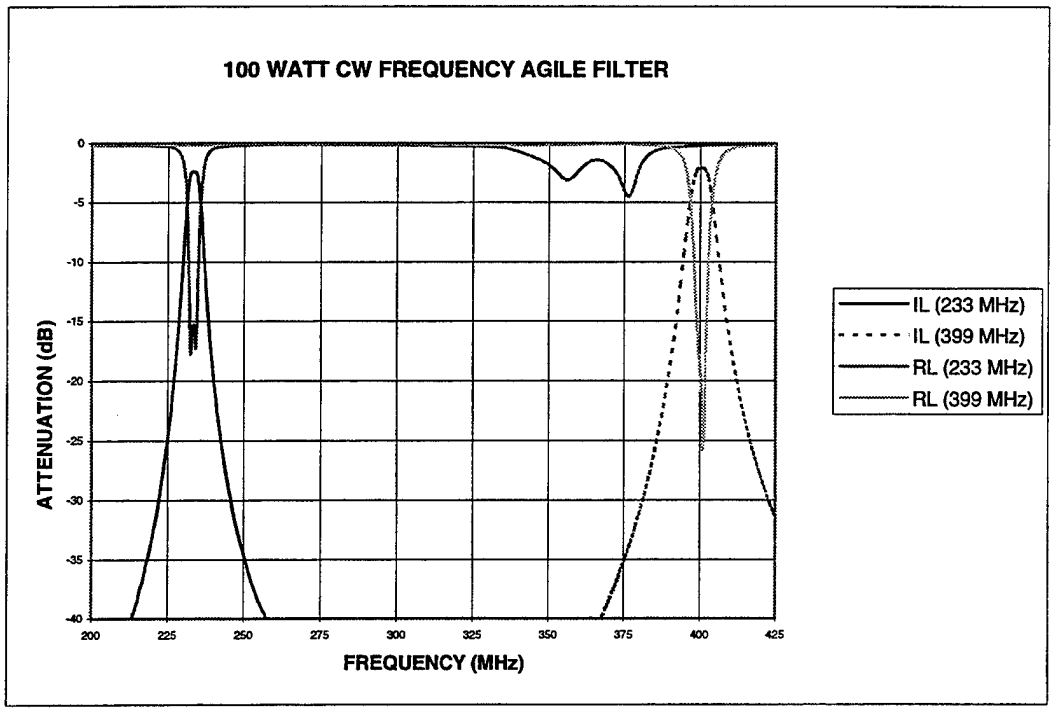

Figure 22. Insertion loss and input return loss versus frequency.

5. CONCLUSIONS AND RECOMMENDATIONS

During the FY 97, wideband distributed-element, high-power circulators and digitally controlled frequency-hopping filters were developed for potential UHF applications. The state-of-the-art distributed circulator prototype has a 1-dB compression at a power level exceeding 1-kW CW with an insertion loss of 0.5 dB. Potentially, this device can be used in various system configurations for both SATCOM and LOS UHF functions under the common aperture concept. Overall, the distributed element approach proves to be more advantageous over the lumped-element approach, especially for multiple-carrier systems. It is recommended that more research be done in miniaturizing the distributed element circulator to make it more practical while enhancing its isolation performance. An additional 10 dB of isolation is needed to implement the aforementioned functions. In addition, improvement of the operational bandwidth to include other system applications up to 2.0 GHz requires further developmental work.

The technology for frequency-hopping filters is not yet fully developed for high-power applications. The current prototype shows impressive power-handling capabilities up to 100 W. Although this is a state-of-the-art device, more tradeoffs between power-handling capabilities and insertion loss need study. A practical filter requires an insertion loss of less than 0.5 dB. Further investigation into various element implementations should improve the power limitation of this technology. The accommodation of current Navy frequency-hopping functions requires the development of a switching circuit for the full 225- to 400-MHz band.

REPORT DOCUMENTATION PAGE

Form Approved
OMB No. 0704-0188

1. AGENCY USE ONLY *(Leave blank)*	2. REPORT DATE	3. REPORT TYPE AND DATES COVERED
	April 1998	Final

4. TITLE AND SUBTITLE
MULTIFUNCTIONAL ANTENNA SYSTEMS FY 97 TECHNOLOGY DEVELOPMENT

5. FUNDING NUMBERS
PE: 0602232N
AN: DN306602

6. AUTHOR(S)
T. Q. Ho, R. C. Adams, W. I. Henry, S. M. Hart

7. PERFORMING ORGANIZATION NAME(S) AND ADDRESS(ES)
Space and Naval Warfare Systems Center
San Diego, CA 92152–5001

8. PERFORMING ORGANIZATION REPORT NUMBER
TD 3027

9. SPONSORING/MONITORING AGENCY NAME(S) AND ADDRESS(ES)
Office of Naval Research
800 North Quincy Street
Arlington, VA 22217–5660

10. SPONSORING/MONITORING AGENCY REPORT NUMBER

11. SUPPLEMENTARY NOTES

12a. DISTRIBUTION/AVAILABILITY STATEMENT
Approved for public release; distribution is unlimited.

12b. DISTRIBUTION CODE

13. ABSTRACT *(Maximum 200 words)*

In FY 97, we conducted two tasks. The objective of the first task was to develop new directive antenna system concepts for satellite communications (SATCOM) applications. The focus of the second task was to develop novel line-of-sight (LOS) antenna concepts and electronics to support the Multifunction Electromagnetic Radiating System Advanced Technology Demonstration (MERS ATD).

14. SUBJECT TERMS
Mission Area: Command, Control, and Communications
radio communications phased-array antenna
multifunction antenna

15. NUMBER OF PAGES
72

16. PRICE CODE

17. SECURITY CLASSIFICATION OF REPORT	18. SECURITY CLASSIFICATION OF THIS PAGE	19. SECURITY CLASSIFICATION OF ABSTRACT	20. LIMITATION OF ABSTRACT
UNCLASSIFIED	UNCLASSIFIED	UNCLASSIFIED	SAME AS REPORT

21a. NAME OF RESPONSIBLE INDIVIDUAL	21b. TELEPHONE *(include Area Code)*	21c. OFFICE SYMBOL
T. Q. Ho	(619) 553–3783 e–mail: tho@spawar.navy.mil	Code D856

INITIAL DISTRIBUTION

Code D0012	Patent Counsel	(1)
Code D0271	Archive/Stock	(6)
Code D0274	Library	(2)
Code D027	M. E. Cathcart	(1)
Code D0271	D. Richter	(1)
Code D80	R. Kochanski	(1)
Code D85	C. J. Sayre	(1)
Code D856	S. M. Hart	(1)
Code D856	T. Q. Ho	(10)

Defense Technical Information Center
Fort Belvoir, VA 22060–6218 (4)

SPAWARSYSCEN Liaison Office
Arlington, VA 22202–4804

Center for Naval Analyses
Alexandria, VA 22302–0268

Navy Acquisition, Research and Development
Information Center (NARDIC)
Arlington, VA 22244–5114

GIDEP Operations Center
Corona, CA 91718–8000